Comparison and evaluation of updates to WRF-Chem (v3.9) biogenic emissions using MEGAN

Mauro Morichetti[1], Sasha Madronich[2], Giorgio Passerini[3], Umberto Rizza[1], Enrico Mancinelli[3], Simone Virgili[3] and Mary Barth[2]

[1]Institute of Atmospheric Sciences and Climate, National Research Council of Italy, Unit of Lecce, Italy
[2]National Center for Atmospheric Research, Boulder, Colorado, USA
[3]Department of Industrial Engineering and Mathematical Science, University of Polytechnic of Marche, Ancona, Italy

Correspondence to Mauro Morichetti (m.morichetti@isac.cnr.it)

Abstract. Biogenic volatile organic compounds (BVOCs) emitted from the natural ecosystem are highly reactive and thus can impact air quality and aerosol radiative forcing. BVOC emission models (e.g., Model of Emissions of Gases and Aerosols from Nature, MEGAN) in global and regional chemical transport models still have large uncertainties in estimating biogenic trace gases, because of uncertainties in emission activity factors, specification of vegetation type, and plant emission factors. This study evaluates a set of updates made to MEGAN v2.04 in the Weather Research and Forecasting model coupled with chemistry (WRF-Chem version 3.9). Our study considers four simulations for each update made to MEGAN v2.04, (i) a control run with no changes to MEGAN; (ii) a simulation with the emission activity factors modified following MEGAN v2.10; (iii) a simulation considering the changes to the plant functional type (PFT) emission factor; and (iv) a simulation with the isoprene emission factor calculated within the MEGAN module instead of prescribed by the input database. We evaluate two regions, Europe and the Southeast United States, by comparing WRF-Chem results to ground-based monitoring observations in Europe (i.e., Airbase database), and aircraft observations obtained during the NOMADSS field campaign. We find the updates to MEGAN v2.04 in WRF-Chem caused overpredictions in ground-based ozone concentrations in Europe and in isoprene mixing ratios compared to aircraft observations in the Southeast US. The update in emission activity factors caused the largest biases. These results suggest that further experimental and modeling studies should be conducted to address potential shortcomings in BVOC emission models.

1 Introduction

Biogenic emissions of volatile organic compounds play a fundamental role in atmospheric chemistry, specifically in the ozone cycle and in the formation of secondary organic aerosols with implications in air quality and climate. The major biogenic volatile organic compounds (BVOCs) are isoprene and monoterpenes (e.g., α, β-pinene) with relative contributions of 69.2 %, and 10.9 %, respectively (Sindelarova et al., 2014). Emissions of BVOC have implications for air quality by affecting the concentration of ground-level ozone (Fehsenfeld et al., 1992; Curci et al., 2010; Sartelet et al., 2012; Sindelarova et al., 2014), and on climate through tropospheric ozone radiative forcing (Brasseur et al., 1998; Gauss et al., 2006). Churkina et al. (2017)

estimated that the impact of BVOC emissions on ground level ozone production was on average 12 % in summer and up to 60 % during a heat wave event in the Berlin-Brandenburg metropolitan area, Germany. With climate change, the increase of isoprene emissions from vegetation due to higher temperatures may lead to higher tropospheric ozone concentrations (EEA, 2015). In addition to the consequences in the gas-phase chemistry, oxidative products of some BVOCs can form secondary organic aerosol (Limbeck et al., 2003; van Donkelaar et al., 2007) with significant effects on the Earth's radiation budget.

The proper quantification of BVOC emitted into the atmosphere is a fundamental parameter in order to represent their effect reliably in global and regional chemical transport models (CTM). Therefore, several modelling approaches have been developed for the estimation of BVOC emissions (Guenther et al., 1995; Niinemets et al., 1999; Martin et al., 2000; Arneth et al., 2007). A fundamental step towards BVOC modelling relates to the work by Guenther et al. (2006) (G06 hereafter), who developed the Model of Emissions of Gases and Aerosols from Nature version 2.0 (MEGAN v2.0) for both regional and global BVOC emission modelling. Several gaps in BVOC emission modelling were addressed in recent releases of MEGAN version 3 and MEGAN version 3.1 (Guenther et al., 2020), including BVOC emissions (i) accounting for sub-grid vegetation distribution in addition to the dominant vegetation type; and (ii) induced by environmental stresses (i.e., extreme weather and air pollution events). Various global and regional-scale chemistry transport models have adopted MEGAN as their BVOC emission model, including the Weather Research and Forecasting model coupled with chemistry (WRF-Chem - Grell et al., 2005; Fast et al., 2006). Zhao et al. (2016) used two versions (v2.04 and v2.1) of MEGAN in order to investigate the sensitivity of WRF-Chem simulated BVOC emissions with different land surface schemes: the Community Land Model version 4.0 (CLM4 - Oleson et al., 2010; Lawrence et al., 2011) and the Noah land surface model (Niu et al., 2011). The land surface schemes quantify land surface processes, their effect on near-surface meteorological conditions, and consequently the simulated BVOC emissions and concentrations. One major difference between the Noah land surface model and CLM4 is that they use different vegetation maps, and this affects BVOC emissions. Zhao et al. (2016) found that BVOC emissions modelled with MEGAN v2.04 were negligible between the two runs with different land surface schemes and the same vegetation map, whereas considering the same land surface scheme with different vegetation maps leads to large differences in simulated BVOC emissions predicted with MEGAN v2.1. Henrot et al. (2017) implemented MEGAN v2.1 in ECHAM-HAMMOZ (ECHAM6 atmospheric general circulation model; HAM aerosol model; MOZART chemistry transport model). Henrot et al. (2017) found the emission factor and PFT distributions most strongly determine the spatial emission distribution in MEGAN in agreement with other previous studies that used different meteorological models (Sindelarova et al., 2014; Messina et al., 2016). Jiang et al. (2019) utilized the WRF-CAMx (WRF meteorology model; CAMx regional air quality model) modelling package to investigate the effect of BVOC emissions on the surface ozone levels in Europe. They found higher (about 3 times) isoprene emissions predicted with MEGAN v2.1 compared to another BVOC emission model (i.e., Paul Scherrer Institute model - Andreani-aksoyoglu and Keller, 1995) resulting in about 10 % higher ozone mixing ratios. Therefore, Jiang et al. (2019) suggested that ozone production occurs generally in VOC-saturated rather than VOC-sensitive regimes in Europe. A few tree species dominate the total isoprene and monoterpene emissions in European forests, with three Quercus species and five types of tree species contributing to 66 and 80 % of total isoprene and monoterpene emissions, respectively (Keenan et

al., 2009). In the work by Wang et al. (2021) the impact of BVOC emissions evaluated with MEGAN version 3.1 on O_3 concentrations simulated with WRF/CAMx varied highly with the drought configurations, with the highest BVOC contribution to ozone concentrations for not including drought stress. Further, because of the complex nature of representing BVOC emissions, previous studies (Messina et al., 2016; Zhang et al., 2021) recommended more measurement campaigns of BVOC emissions to validate BVOC model results.

As noted above, Zhao et al. (2016) have implemented MEGAN v2.1 in WRF-Chem with the CLM4 land model; CLM surface scheme and associated subroutines in the physics and chemistry packages have been modified to be consistent with the MEGAN v2.1 biogenic emission. These changes became part of the community version of WRF-Chem in 2021 with the release of WRF version 4.3. In our work, which we performed before WRF version 4.3 was available, we use WRF-Chem version 3.9, to explore the effect of making changes to the existing WRF-Chem MEGAN v2.04 emissions scheme. Because we modified the MEGAN v2.04 code, our method results in having changes that can be used with the Noah land surface model. In section 2, we describe the changes that were made to MEGAN v2.04.

To compare different updates to MEGAN v2.04 introduced by G12 with MEGAN v2.10 in simulating BVOC emissions, two case studies were performed in two different domains (i.e., Europe and the Southeast United States). Since ozone is known to be a result of photochemistry involving nitrogen oxides (NO_X = NO + NO_2) and volatile organic compounds (VOC), a sensitivity study on BVOC emissions was performed for a high-ozone episode in August 2015 in Europe considering different updates to MEGAN v2.04 introduced with MEGAN v2.10. For this case study, comparisons are presented between modelled ozone concentrations and surface measurements (AirBase database - https://www.eea.europa.eu/data-and-maps/data/aqereporting-9). Summer 2015 was among the six hottest and driest summers since 1950 in Europe (Ionita et al., 2017). These meteorological conditions together with 4 heatwave episodes led to high tropospheric ozone levels throughout Europe, with 18 of the EU-28 countries exceeding the EU ozone threshold value for the protection of human health (EEA, 2017). Lin et al. (2020) have reported a link between ozone episodes in Europe and the ecosystem-atmosphere interactions during heatwaves and droughts, with lower ozone uptake by water-stressed vegetation exacerbating the peak ozone events. For the Southeast United States case study, BVOC emissions calculated with MEGAN v2.04 and MEGAN v2.10 were evaluated against aircraft measurements. The measurements of isoprene, two products of isoprene oxidation (i.e., methacrolein, and methyl vinyl ketone) and ozone were taken in five of the research flights under the Southern Oxidant and Aerosol study (SOAS) in June 2013. The SOAS project is part of the Nitrogen, Oxidants, Mercury and Aerosol Distributions, Sources and Sinks (NOMADSS) project (https://www.eol.ucar.edu/field_projects/nomadss) under the umbrella of Southeast Atmosphere Study (SAS - https://data.eol.ucar.edu/project/SAS), a project aimed at investigating the interactions between atmosphere and biosphere and the role of BVOC in atmospheric chemistry in the Southeast and Central United States. A synthesis of relevant results achieved within SAS was presented by Carlton et al. (2014). Section 3 describes these two cases in more detail and the WRF-Chem v3.9 configurations to represent the two cases. In section 4, the effects of specific updates to the MEGAN v2.04 model are examined and evaluated with observations from each of the case studies. A summary and conclusions are given in section 5.

2 Materials and Methods

The MEGAN model estimates the emissions considering meteorology (e.g., temperature, solar radiation, and soil moisture), leaf area index (LAI), and PFT as driving variables, with higher emissions occurring for higher values of temperature, transmission of photosynthetic photon flux density, and LAI. MEGAN v2.0 was used for analyzing the impact of biogenic emissions with potential future increases in ambient temperature on ozone levels (Im et al., 2011), aerosol levels and chemical compositions (Im et al., 2012). Building on MEGAN v2.0 (G06) and MEGAN v2.02 (Sakulyanontvittaya et al., 2008), Guenther et al. (2012) (G12 hereafter) introduced additional compounds, emission types, and controlling processes with MEGAN v2.1. In MEGAN v2.1, the emission factors are adjusted to consider that the measured net flux of BVOC compounds above the vegetation canopy does not involve the dry deposition flux, so that the net primary emissions would be higher (e.g., up to a few percent for isoprene). To better depict the variability of isoprene emission within a PFT category, MEGAN v2.1 allows specific PFT emission factors for each vegetation type.

2.1 Updates to MEGAN v2.04 in WRF-Chem

The Model of Emission of Gases and Aerosols from Nature (MEGAN) model estimates the net emission rate of 134 chemicals species (e.g. isoprene, monoterpenes, oxygenated compounds, sesquiterpenes and nitrogen oxide) from terrestrial ecosystems into the above-canopy atmosphere with a resolution of 1 km^2 (G06). MEGAN can be used in both global models, such as GEOS-Chem (Goddard Earth Observing System) (Bey et al., 2001) or CAM-Chem (Community Atmosphere Model) (Tilmes et al., 2015; Lamarque et al., 2012), and regional CTM, such as WRF-Chem (Grell et al., 2005; Fast et al., 2006).

The BVOC emission algorithm currently applied to WRF-Chem is calculated as follows:

$$EM = \varepsilon \cdot \gamma_P \cdot \gamma_T \cdot \gamma_{age} \cdot \gamma_{SM} \cdot \gamma_{LAI} \cdot \rho, \quad (1)$$

where EM is the BVOC emission rate (μg m^{-2} hr^{-1}); ε the emission factor (μg m^{-2} hr^{-1}); γ_P, γ_T, γ_{age}, γ_{SM} and γ_{LAI} are the emission activity factors that account respectively for photosynthetic photon flux density, temperature, leaf age, soil moisture and LAI (normalized ratio); and ρ the loss and production within plant canopy (normalized ratio). The emission rate (EM) is calculated for each PFT, added up to estimate the total emission at each model grid cell, and corrected considering the deviation from the standard condition (γ and ρ parameters). The factor γ and ρ are equal to unity at standard conditions (e.g., air temperature 303 K, specific humidity 14 g kg^{-1}, wind speed 3 m s^{-1}, and soil moisture 0.3 m^3 m^{-3}), while they are different from unity with no-standard conditions (G06).

Note that this work simply replaces equations in the MEGAN v2.04 code with the equations in MEGAN v2.10. Table 1 lists the equations from MEGAN 2.04 with what they were replaced with from the MEGAN v2.10 paper (G12). One difference between this work and that of G12 is that this paper retains four plant functional types while G12 use 15 plant functional types. Details on the update of emission factors for this paper are given in section 2.3.

In the present study, we made four simulations with the following configurations. (i) The control run with no changes (M2.04). (ii) The updates to the emission activity factors (i.e., gamma equations for LAI, PPFD, temperature, soil moisture and canopy

environment), following G12 paper (MG). (iii) The updates to the emission factor for 4 PFT (MGPFT). With this simulation we had two effects, firstly α-pinene emissions changed from the MG simulation to the MGPFT simulation, and secondly isoprene emissions did not change from the MG to the MGPFT simulation. In the MGPFT simulation, the changes to PFT emission factor and PFT percentage, in the code, did not affect isoprene as its emission factor was considered directly from the pre-processor MEGAN. (iv) We forced the code to calculate the isoprene emissions as the other compounds were determined, instead of directly reading the value of emission factor from the database as in the previous simulations. This resulted in isoprene emissions changing from previous simulation (i.e., MGPFTISO different from MGPFT), while α-pinene remained the same (i.e., MGPFTISO identical to MGPFT).

2.2 Update of the emission activity factors

Emission activity factors describe variations in BVOC emission related to physiological and phenological processes. The capability of a leaf to emit isoprene depends on a number of physical and biological factors, with incident photosynthetic photon flux density and leaf temperature as driving factors (Guenther et al., 1993). A leaf's capacity to emit isoprene is also influenced by leaf phenology, with very-young leaves emitting no isoprene and mature leaves emitting isoprene maximally. Moreover, soil characteristics play a role in the plants BVOC emission ability, with droughts significantly decreasing isoprene emission (G06; Jiang et al., 2018).

The integration of MEGAN with CTMs parameters (e.g., temperature, solar radiation, and soil moisture) allows an improved analysis of interactions between BVOC emissions, the surrounding environment, and the canopy itself. The standard MEGAN environment model is based on the methods described by Guenther et al. (1999) who estimated incident PPFD and temperature at five canopy depths, including a leaf isoprene-emitting model driven by humidity, solar radiation, ambient temperature, and soil moisture. Overall, the BVOC emissions are a product of both the local weather at the time of simulation (i.e., temperature, humidity, and PPFD), and long-term conditions, such as the conditions over the past month (i.e., based on seasonal conditions like soil moisture and heat waves or drought). Therefore, the emissions are a function of both the instantaneous temperature and the temperature averaged over 1–10 days. Several algorithms have been widely used to simulate the response of isoprene emission to changes in light, temperature, leaf age and soil moisture (Guenther et al., 1995, 1999, 1993). However, complexity and expensive computational costs hindered their use in CTMs. To minimize computational costs, G06 developed a parameterized canopy environment emission activity (PCEEA) algorithm as an alternative to calculating all variables at each canopy. The PCEEA procedure includes algorithms for the solar radiation, temperature, and canopy environment response emission activity factors (i.e., γ_P, γ_T and γ_{LAI}) in MEGAN v2.04.

2.2.1 Light response emission activity factor

One of the main advances introduced with MEGAN v2.10 is that the emission activity factors of each compound class comprised of a light-dependent fraction (LDF) and a light-independent fraction (LIF). MEGAN v2.04 calculates the light response emission activity (γ_P) using the sine of the solar angle with no distinction between the light dependent and independent

fractions (Eq. from (10) to (13) of G06) (Table 1). For each compound class, the updated emission activity factor is calculated for the PPFD variations as follows:

$$\gamma_{P,i} = (1 - LDF_i) + LDF_i \cdot \gamma_{P\_LDF}, \quad (2)$$

$$\gamma_{P_{LDF}} = C_P \left[\frac{\alpha \cdot PPFD}{(1+\alpha^2 \cdot PPFD^2)^{0.5}}\right], \quad (3)$$

$$C_P = 0.0468 \cdot e^{(0.0005 \times [P_{24} - P_S])} \cdot [P_{240}]^{0.6}, \quad (4)$$

$$\alpha = 0.004 - 0.0005 \cdot \ln(P_{240}), \quad (5)$$

where the PPFD is the instantaneous photosynthetic photon flux density (μmol m^{-2} s^{-1}); the Ps standard conditions for PPFD averaged over the past day (200 μmol m^{-2} s^{-1} for sun leaves and 50 μmol m^{-2} s^{-1} for shade leaves); P_{24} is the average PPFD of the past 24 hours; the P_{240} is the average PPFD of the past 10 days (Table 1). The version 2.10 calculates the γ_P with the photosynthetic photon flux density using the internal variable "swdown": the downward solar radiation (W m^{-2}). P_{24} and P_{240} are the average PPFD of the past day and the past ten days, nevertheless they are both equal to "mswdown" variable: the downward solar radiation (W m^{-2}) of previous month (G12).

2.2.2 Temperature response emission activity factor

In MEGAN v2.04, the temperature activity factor (γ_T) calculates the response emission activity for isoprene according to Eq. (5), Eq. (8), and Eq. (15) by G06; all the others non-isoprenoid compounds are described according to the monoterpene exponential temperature response function by Guenther et al. (1993).

The updated temperature activity factor (MEGAN v2.10) leads to two different changes, (i) the introduction of LDF and LIF (i.e., as the previous emission factor), and (ii) the dependency on the specific class compounds instead of the isoprene and non-isoprene species. The updated version of LDF of temperature activity factor (γ_T) is calculated as follows:

$$\gamma_{T,i} = (1 - LDF_i) \cdot \gamma_{T\_LIF,i} + LDF_i \cdot \gamma_{T\_LDF,i}, \quad (6)$$

$$\gamma_{T_{LDF,i}} = E_{opt} \cdot \left[CT_2 \cdot \frac{e^{(CT_{1,i} \cdot x)}}{CT_2 - CT_{1,i} \cdot (1 - e^{(CT_2 \cdot x)})}\right], \quad (7)$$

$$x = \frac{\left[\left(\frac{1}{T_{opt}}\right) - \left(\frac{1}{T}\right)\right]}{0.00831}, \quad (8)$$

$$E_{opt} = C_{eo,i} \cdot e^{(0.05 \cdot (T_{24} - T_S))} \cdot e^{(0.05 \cdot (T_{240} - T_S))}, \quad (9)$$

$$T_{opt} = 313 + \left(0.6 \cdot (T_{240} - 297)\right), \quad (10)$$

where E_{opt} is the maximum normalized emission capacity (mol km^{-2} hr^{-1}); T_{opt} the temperature at which E_{opt} occurs (K); T is the leaf temperature (K) assumed to be the air temperature at 2 m (=T2) calculated by WRF at each grid point; $CT_{1\text{-}i}$, CT_2, and $C_{eo\text{-}i}$ are emission-class dependent empirical coefficients; T_s the standard conditions for leaf temperature (297 K); T_{24} the average leaf temperature of the past 24 hours (K); T_{240} the average leaf temperature of the past 240 hours (K).

The response of LIF is determined according to the monoterpene exponential temperature response function by Guenther et al. (1993):

$$\gamma_{T_{LIF,i}} = e^{(\beta_i(T-T_S))}, \quad (11)$$

where β_i is an empirically determined coefficient, depending on the emission compound class (G12).

Additional changes made on this part of the code concern the update of the CT_1, CT_2 and C_{eo} parameters. In G06 their values are set respectively to 80, 200 and 1.75, whereas $CT_{1,i}$ and $C_{eo,i}$ depend on the classes compound, and CT_2 still have a fixed value (i.e., 230) in the updated version (Table 1). A more accurate BVOC evaluation with each compound class having the appropriate value may result from (i) the temperature activity factor defined as the weighted average of a light dependent and independent fraction ($\gamma_{Ti,LDF}$ and $\gamma_{Ti,LIF}$), (ii) and the update of the model parameters (CT_1, CT_2, and C_{eo}), for each compound class. Note that the value of T_{24} and T_{240} are estimated equal to the variable monthly surface air temperature (MTSA) with MEGAN v2.10. Therefore, it is assumed that the average temperature of the past 24 hours, and the past ten days, are the same as the average temperature of the past month ($T_{24} = T_{240} = MTSA$).

2.2.3 Leaf age response emission activity factor

The canopy isoprene-emitting capability is also influenced by the leaf age. An increase in foliage is assumed to imply a growing production of isoprene (young leaves), whereas decreasing foliage is associated with less production of isoprene (old leaves). Guenther et al. (1999) developed an algorithm, with a time step of one month, to simulate the emissions change for young, mature, and old leaves. The algorithm adapted to MEGAN v2.04 assumes a constant value ($\gamma_{age}=1$) for evergreen canopies, while deciduous canopies are divided into four fractions: new foliage (F_{new}), growing foliage (F_{gro}), mature foliage (F_{mat}) and old foliage (F_{old}). The leaf age factor is computed as

$$\gamma_{age} = F_{new}A_{new} + F_{gro}A_{gro} + F_{mat}A_{mat} + F_{old}A_{old}, \quad (12)$$

where A_{new}, A_{gro}, A_{mat}, and A_{old} are the relative emission rates assigned to each canopy fraction depending on PFT categories. The canopy is divided into leaf age fractions based on the change in LAI between the current time step (current month = LAI_c) and the previous time step (previous month = LAI_p). The difference between the two LAI values describes the leaf area index age. No difference in LAI (i.e., $LAI_p=LAI_c$) indicates a canopy mostly formed by mature foliage. A canopy is formed by old foliage when the LAI value of previous month is greater than the one in the current month ($LAI_p>LAI_c$), whereas $LAI_p<LAI_c$ for a canopy primarily formed by new foliage (G06).

MEGAN v2.10 estimates the leaf age emission activity factor (γ_{age}) in Eq. (12) based on the same calculations described by Eq. (16) in G06. The two versions of MEGAN do not differ for the canopy subdivision into four fractions (i.e., new foliage (F_{new}), growing foliage (F_{gro}), mature foliage (F_{mat}), and old foliage (F_{old})) and the related computation. The only update of equation parameters is the relative emission rates assigned to each compound class (A_{new}, A_{gro}, A_{mat}, and A_{old}) reported in Table 4 of G12 (**Error! Reference source not found.**Table 1).

2.2.4 Soil moisture response emission activity factor

Different studies have shown that isoprene emission decreases when soil moisture drops below a threshold, and eventually becomes insignificant, when plants are exposed to extended drought (Jiang et al., 2018; Pegoraro et al., 2004). In the WRF-Chem version of MEGAN v2.04, the soil moisture activity factor (γ_{SM}) is set to 1.0 for both isoprene and no-isoprene classes compound. Therefore, the soil moisture dependence is not involved into the BVOC emissions algorithm. In the present study, (in MEGAN v2.10 code applied to WRF-Chem), isoprene emissions were evaluated according to the Eqns. (20-a), (20-b) and (20-c) described by G06 as follows:

$$\gamma_{SM,isoprene} = 1 \qquad (\theta > \theta_1) \tag{13}$$

$$\gamma_{SM,isoprene} = \frac{\theta - \theta_W}{\Delta\theta_1} \quad (\theta_W < \theta < \theta_1) \tag{14}$$

$$\gamma_{SM,isoprene} = 0 \qquad (\theta < \theta_W) \tag{15}$$

$$\theta_1 = \theta_W + \Delta\theta_1 \tag{16}$$

where θ is soil moisture ($m^3\ m^{-3}$); θ_w is the soil moisture threshold below which plants cannot extract water from soil (wilting point, $m^3\ m^{-3}$); $\Delta\theta_1$ (=0.06) is an empirical parameter from Pegoraro et al. 2004. MEGAN uses a wilting point database that assigns different θ_w values for each soil type based on Table 2 of Chen and Dudhia (2001) (Table S1 of supplemental materials). Since for G12 the non-isoprenoid soil moisture dependence is not involved into the BVOC emissions algorithm, in the present study, the γ_{SM} for non-isoprenoid compounds is still set to 1.0.

2.2.5 Canopy environment response emission activity factor

The emission response to leaf area index (γ_{LAI}) in MEGAN v2.04, calculates the response emission activity factor by Eq. (15) of G06. In MEGAN v2.10 the canopy environment coefficient has been simplified as follows:

$$\gamma_{LAI} = LAI \cdot C_{CE}, \tag{17}$$

where LAI ($m^2\ m^{-2}$) is the leaf area index referred to the month of the simulation; C_{ce} is a value dependent on the canopy environment model being used. WRF-AQ (Weather Research Forecast – Air Quality) canopy environment model uses a value of 0.57 (G12).

2.3 Updates of PFTs and isoprene emission factors

An important difference between MEGAN v2.04 and MEGAN v2.10 is the number of PFTs described and the associated isoprene emission factors. Only four PFTs are used in MEGAN v2.04, including Needleleaf Trees, Broadleaf Trees, Broadleaf Shrubs, and Grass and other. In contrast, MEGAN v2.10 includes 15 PFTs (Needleleaf Evergreen Temperate Tree, Needleleaf Evergreen Boreal Tree, Needleleaf Deciduous Boreal Tree, Broadleaf Evergreen Tropical Tree, Broadleaf Evergreen Temperate Tree, Broadleaf Deciduous Tropical Tree, Broadleaf Deciduous Temperate Tree, Broadleaf Deciduous Boreal Tree, Broadleaf Evergreen Temperate Shrub, Broadleaf Deciduous Temperate Shrub, Broadleaf Deciduous Boreal Shrub, Arctic C3

Grass, Cool C3 Grass, Warm C4 Grass and Crop). In order to explore the effect of the updated emission factors without revising the pre-processing code, we opted to apply a typical emission factor from G12 (Table 2) to the four PFTs currently in WRF-Chem. Table 2 shows the updated emission factors for the four PFTs, and their previous value from MEGAN v2.04. The new isoprene emission factor decreased, for all PFT, except for herbaceous species (HB - Grass and other); at the bottom of Table 2 it is noticeable that carbon monoxide, the bidirectional, the stress and the other VOC decreased with new values, independently the PFT considered. For all the other classes compound, the new emission factors are larger than the previous emission factors.

The PFTs emission factors update does not change the isoprene emission, as its emission factors in MEGAN v2.04 implemented in WRF-Chem are estimated directly from the input database. Thus, a sensitivity simulation was performed with the isoprene emission factor evaluated according to the MEGAN emission algorithm Eq. (1), instead of the input database as outlined in section 3.

3. Case Study Descriptions and Model Configuration

3.1 European Case

3.1.1 Characterization of Case from Observations

Summer 2015 was among the six hottest and driest summers since 1950 in Europe (Ionita et al., 2017). In this year, high tropospheric ozone episodes were experienced throughout Europe, with 18 of the EU-28 countries as well as 41 % monitoring stations reporting the ozone maximum daily eight-hour mean above 120 μg m^{-3} (=60.4 ppb; the current target value for ozone in Directive 2008/50/EC) on more than 25 days (EEA, 2017). Therefore, a 6-day high ozone period (10–16 August 2015) was selected to evaluate the impact of the changes in the MEGAN v2.04 scheme on isoprene emissions and ozone mixing ratios.

The high ozone levels were confirmed by examining the summertime (May–September) hourly average ozone concentrations measured at the air-quality monitoring stations in Marche region (Italy) (Figure 1-a and Figure 1-b), over a period of 3 years (from 2013 to 2015). The analysis results indicate that an extraordinary ozone peak event occurred in the time period 10–16 August 2015.

3.1.2 Model Configuration

On August 13th, all the air quality stations (i.e., Marche region air quality stations), reported the highest ozone daily eight-hour mean concentration value of the whole year (Figure 1-c). To represent the evolution of ozone peak event the simulations lasted 6 days, from August 10th (00:00 UTC) to August 16th (00:00 UTC), with 2 days of spin up for the model. A spin up time of 48 h is used for the chemistry to be consistent with the ambient conditions following past studies (Yerramilli et al., 2012; Zhang et al., 2009). The initial domain configuration used a nested domain over Italy with a 4x4 km grid, but instead of

focusing over the Marche region of Italy, we analyse the larger domain over Europe to explore the capabilities of the updated MEGAN algorithm for different vegetation types and chemistry regimes.

The WRF-Chem model (simulation domain showed in the Figure 2) used initial and boundary conditions from the FNL (Final) Operational Global Analysis data (Ncep, 2000). These data are available every six hours on a (1° x 1°) spatial grid. As summarized in Table 3, the following physical schemes were used. The Morrison double-moment scheme was selected for the treatment of the microphysics processes (Morrison et al., 2009). The Rapid Radiative Transfer Model (RRTMG), for both shortwave and longwave radiation is used; this allows to activate the aerosol direct radiative effect (Iacono et al., 2008), to represent scattering and absorption in the atmosphere. The Mellor-Yamada-Janjic (MYJ) parameterization was considered to describe the planetary boundary layer (Janjić, 1994). The unified Noah land-surface model was chosen to represent the land surface interaction (Chen et al., 1996). It includes soil temperature and moisture in four layers, fractional snow cover and frozen soil physics. The Grell-Freitas scheme was considered for the cumulus parameterization scheme: it tries to smooth the transition to cloud-resolving scales (Grell and Freitas, 2014).

To investigate the role of isoprene on the high ozone event recorded in Europe, the selected chemical package was the chemical option with the Model for Ozone and Related chemical Tracers (MOZART) version 4 (Emmons et al., 2010) for the trace gases, and the Model for Simulating Aerosol Interactions and Chemistry (MOSAIC) (Zaveri et al., 2008) for the aerosol-phase species. The CAM-chem (Tilmes et al., 2015; Lamarque et al., 2012) global model results are used for the chemical initial and boundary conditions for both the gas and aerosol components. The Emission Database for Global Atmospheric Research-Hemispheric Transport of Air Pollution (EDGAR-HTAP) emission inventory for Europe provided the anthropogenic emissions (Janssens-Maenhout et al., 2012). The open biomass burning emissions were from the Fire Inventory from NCAR-FINN model (Wiedinmyer et al., 2011) and the biogenic emissions from the MEGAN database (G06, G12).

Table 4 lists the four simulations conducted to study the MEGAN updates described above. The control run (M2.04) uses the MEGAN v2.04 database without any changes. The second simulation (MG) includes only the changes to the activity factors (γ). The third simulation (MGPFT) adds to the changes in the activity factors the variation of the PFTs emission factors (listed in Table 2). The fourth simulation (M2.10) is the same as the MGPFT run, except the isoprene emission factor is calculated with Eq. (1) instead of prescribed by the input data.

3.2 Southeast US Case

3.2.1 Characterization of Case from Observations

The NOMADSS project, which SOAS was part of, took place over the southeastern United States from June 1st to July 15th, 2013. The NSF/NCAR C-130 flight tracks covered much of the eastern United States. The NOMADSS field campaign includes 19 flights from June 3rd to July 14th, 2013. For these flights, the aircraft sampled air in isoprene-rich emissions regions (Figure 3). Specifically, the flight tracks had high isoprene mixing ratios when the aircraft was in the boundary layer. The low isoprene mixing ratios occurred when the aircraft was above the boundary layer. For example, this trend can be observed in the time

series of flight altitude (Figure 17-a) and measured isoprene concentration (Figure 17-c, black markers) for the second NOMADSS flight (rf02).

3.2.2 Model Configuration

Figure 4 shows the model domains. The coarse domain has 442×265 grid points with 12 km grid cells centered at 40° N 97° W, covering the United States of America (USA) (CONUS domain – SW corner 22.83° N 120.49° W; NW corner 52.46° N 136.45° W; NE corner 45.98° N 60.82° E; SE corner 20.08° N 81.24 W). The nested domain is centered over the southeastern area of the USA with 301×301 grid points and 4 km grid cells including the selected NOMADSS flight tracks (rf01 - rf05) inside the simulation domain. Both domains consider 40 vertical levels up to 50 hPa. The simulations lasted 14 days, from June 1st (00:00 UTC) to June 15th (00:00 UTC), 2013. The simulations started two days before the first flight (rf01 - June 3rd) so as to guarantee a spin up for the model (Yerramilli et al., 2012; Zhang et al., 2009). To compare directly with the aircraft measurements, the "tracking" option was selected in WRF-Chem. This option outputs the vertical profiles of prescribed meteorological and chemical species at a set of prescribed times and horizontal coordinates, taken from the location and time of the aircraft.

Meteorological boundary and initial conditions were extracted from NCEP North American Regional Reanalysis (NARR – ds608.0). The NARR project is an addition to the NCEP global reanalysis which is run only over the North American Region with the 32-km grid spacing of NCEP Eta model (NCAR, 2005). The configuration of the physical and chemical/aerosol schemes used for this part of the study is the same as that described in the previous section and reported in Table 3. Two simulations were performed to evaluate the MEGAN model updates with the measurements sampled by the NCAR C-130. The two simulations were M2.04, with the original MEGAN v2.04 database, and M2.10 with all the code updates described previously in sections 2.2 and 3.1.

4. Results

4.1 European Case Study

In this section, we begin by describing and evaluating the synoptic meteorological conditions for August 10-15, 2015, as well as evaluating WRF-Chem temperature predictions with ground-based measurements, because isoprene emissions depend strongly on temperature. Then we show how isoprene and α-pinene emissions differ among the four simulations (M2.04, MG, MGPFT, and M2.10). Lastly, since BVOC observations are not available, trace gas (NO_x, CO and O_3) concentrations are compared between the different simulation concentration outputs with ground-based observations. The evaluation is conducted with both a statistical analysis based on the calculation of mean-bias, correlation coefficient and normalized root mean square error, and an assessment of the spatial distribution of the NO_x, CO and O_3 concentrations.

4.1.1 Synoptic conditions

We begin with evaluating the synoptic conditions predicted by the WRF-Chem simulations. The 6-day average geopotential height map at 850 hPa (Figure 5-a), shows the presence of an intense geopotential height maximum (1520–1580 m), affecting the central part of the Mediterranean basin, in steady-state for the duration of the period analyzed. The ridge separates a geopotential height minimum (1300–1340 m) over north-western Europe from a weak depression (1460–1500 m) over Turkey. As a consequence, central and southern Europe are affected by north-easterly currents from north Europe, allowing the weak depression to cross Italy toward the southeast portion of the domain. The WRF-Chem (Figure 5-b), simulations are consistent with the evolution represented in the reanalysis, although with some slight differences. In particular, the low pressure is more intense in the WRF-Chem runs, whereas the high-pressure across Italy is more intense in the NCAR/NCEP reanalysis. Comparison between simulated (Figure 5-a) and observed (Figure 5-b) 6-day average temperature shows that the values and the spatial distribution of temperature are well depicted by WRF-Chem model. The lowest temperatures (i.e., 5–10 °C) are in north-western Europe (i.e., Iceland). Temperatures increase in the north-easterly direction with values in the range of 10–15 °C in most parts of England and the Scandinavian Peninsula. Along the central and western Europe, the temperature increases up to 15–25 °C (e.g., Portugal, Spain, French, Germany). Southeast Europe (e.g., Italy, Croatia, Albania, Greece, and Turkey) has the highest temperatures up to about 30–35 °C.

Examination of the downward short wave radiation flux and total precipitation for the four simulations showed that these parameters do not change with the variation of the BVOC emissions (Figure S1 and Figure S2 in supplement material). The ozone feedbacks do not influence the solar radiation as the ozone considered from the radiation scheme (i.e., RRTMG from Iacono et al., 2008) is a default value, and not the value calculated in the code algorithms. Even the total precipitation does not change between simulations as we did not include aerosol-cloud interactions in the simulations.

4.1.2 Examination of the MEGAN emission algorithm updates

The map of PFTs percentage coverage reveals higher coverage of needleleaf trees compared to broadleaf, and shrub and bush in north-eastern Europe with values between 30–70 % and, with comparable trend, in the north of Spain (i.e., the Cantabrian Mountains), Italy (i.e., Alps), Germany and in the most part of the Balkans peninsula (i.e., Carpathian Mountains) (Figure 6 a-d). The Broadleaf coverage has a geographical distribution similar to the Needleleaf trees, but with lower values (from 10 to 40 %). The shrub and bush PFT are predominant in Norway, north of Russia, south-eastern part of Spain, and Turkey. The Herbs cover the greatest portion of central Europe with a value 70-100 %, since there is a substantial number of plants that fall within this plant functional type (Grass and other - PFTP_HB). The isoprene emitting genera in this category include: Phragmites (a reed), Carex (a sedge), Stipa (a grass) and Sphagnum (a moss) (G06).

Four European cities, Porto (Portugal), Genoa (Italy), Zagreb (Croatia), and Kiev (Ukraine) shown in Figure 2, were selected for analyzing the time series of isoprene and α-pinene emissions. These four cities represent warmer to cooler conditions experienced over Europe and are located in areas characterized by different PFTs (Figure 6). Figure 7 (a-d) shows the time

series of isoprene emissions in the four selected cities from 10th to 16th August 2015. The isoprene diurnal cycle responds to the daily fluctuations in solar radiation. The updates applied to MEGAN v2.04 in WRF-Chem resulted in increased isoprene emissions of up to 3 times for each city analyzed. Modifying the gamma factors (MG simulation) produced the greatest increase in emissions, while modifying the PFT emission factors with isoprene emission factors obtained from the input database (MGPFT) produced the same emissions magnitude as the MG simulation. Applying calculated isoprene emission factors (M2.10) gave lower isoprene emissions than MG and MGPFT, but still higher emissions than M2.04. The magnitude of the isoprene emissions varied between cities where simulated isoprene emissions ranked as follows: Zagreb > Porto > Genoa > Kiev. Differences in the isoprene emission magnitudes are caused by the plant functional types in each city and their respective emission factors. For example, Zagreb has about 30 %, 40 %, 20 %, and 70 % for BT, NT, SB, and HB vegetation, respectively, while Kiev has about 10 %, 30 %, 20 %, and 90 % for BT, NT, SB, and HB vegetation, respectively (Figure 8). Temperature and cloudiness can play a role in isoprene emission magnitude too. Figure 5 shows the temperature across Europe. Porto has the temperature in the range of 20-25 °C, Zagreb 25-30 °C, Genoa 20-25 °C and Kiev 15-20 °C. Also, Porto and Genoa and possibly Kiev look like they may have experienced cloudiness based on the shape of the diurnal profile. On clear sky days, the isoprene emissions diurnal profile is smooth with a peak at midday. Clouds that form during the day can attenuate the solar radiation affecting the gamma-light parameter in the MEGAN calculation. In Figure 7, the more jagged diurnal profiles of isoprene emissions are likely due to cloudiness at different times of day.

Figure 9 (a-d) shows the time series of α-pinene emissions for the selected cities from August 10th to August 16th, 2015. Among the monoterpene compounds, α-pinene is the highest contributor to the global annual BVOC emissions (Henrot et al., 2017). In each city, α-pinene emissions show daily patterns with peaks in the daytime and plateaus in the night-time, as with the isoprene emissions but with an order of magnitude lower. In each of the cities analyzed, the simulated α-pinene emissions ranked as follows: MGPFT ≡ M2.10 > MG > M2.04. The α-pinene emissions from the MGPFT are the same as those from the M2.10 simulation, since the M2.10 code introduces only changes to isoprene emissions. As with the isoprene emissions, the updates to the gamma factors (MG) produced the greatest change in emissions, while modifying the emission factors (MGPFT) increased emissions somewhat more than the MG simulation. This result is consistent with the 10-20 % increase in emission factors for NT and SB vegetation (Table 2). In general, the α-pinene emission values increase between 0.5 mol km^{-2} hr^{-1} (Kiev – 5th day) to 10 mol km^{-2} hr^{-1} (Porto – 1st day) compared to the control simulation (i.e., M2.04). As with isoprene, the differences in the α-pinene emission magnitudes are caused by the plant functional types, temperature, and cloudiness for each city (Figure 10).

Figure 11 and Figure 12, illustrate the spatial distribution of BVOC emissions calculated with different MEGAN configurations, respectively for isoprene and α-pinene emissions, as the weekly averaged emission flux (from August 10th 00:00 UTC to 16th 00:00 UTC, 2015). The updates to the MEGAN algorithm introduce a significant increase in both isoprene and α-pinene emissions. The areas with higher increases (from 15 to 50 mol km^{-2} hr^{-1} for isoprene emissions; from 0.5 to 5 mol km^{-2} hr^{-1} for α-pinene emissions) in emissions are the Balkan Peninsula, the Apennine Mountains (Italy), and part of the Black Sea coasts (Turkey and Georgia). The Iberian Peninsula and central-east Europe show minor differences, but still noteworthy

(from 15 to 35 mol km^{-2} hr^{-1} for isoprene; from 0.5 to 3.5 mol km^{-2} hr^{-1} for α-pinene). The increase of emissions on the Balkan Peninsula, Italy, and Black Sea coast are likely a result of the substantial increase in γ_{LAI} (Figure S3), which contrasts with the decreased Broadleaf PFT emission factor from 13000 to 9000 μg m^{-2} hr^{-1} (Table 2).

In Figure 14 (a-d), a comparison is presented between M2.04 run (green points) and the M2.10 (red points) emission activity factors γ_P, γ_T, γ_{age}, and γ_{LAI} for the city of Genoa (Italy) on August 13th (12:00 UTC) 2015 (Figure S3, Figure S4 and Figure S5, of supplement material, show the remaining emission activity factors, respectively, for Kiev, Porto and Zagreb). The new emission activity factors are substantially higher than those in MEGAN version 2.04. The PPFD gamma factor increases for isoprene from 1.25 in M2.04 to 2.3 in M2.10, which is 1.8 times greater, and for α-pinene from 1.0 to 1.2. While isoprene and other VOCs had little change in the temperature gamma factor (gamma_T); the γ_T factor increased from 1.0 for M2.04 to 1.6 for M2.10. The leaf age emission activity factor (gamma_A) changed <10 % between M2.04 and M2.10, decreasing for isoprene and increasing for α-pinene. For all VOCs, the LAI gamma factor increased from 0.9 to 1.7, which has a substantial effect on the VOC emissions. Figure 15 (a-d) shows the total emission activity factors (i.e., gamma = gamma_P*gamma_T* gamma_A*gamma_LAI) for each city between version 2.04 (M2.04, green points) and version 2.10 (M2.10, red points) of MEGAN equation for 12:00 UTC August 13, 2015. Compared to the M2.04 run, the emission activity values have increased significantly in the M2.10 run even considering the total value with an average value of about: 3 (Genoa and Zagreb), 0.6 (Porto), and 0.45 (Kiev). Naturally the increase of total values derives from the variation of single activity factors, for example in Genoa the values double by updating the code from M2.04 to M2.10, particularly for γ_P, γ_T and γ_{LAI} (Figure 15); Zagreb shows a similar trend. The gap relative to Kiev and Porto instead, is mainly due to γ_T and γ_{LAI}, while the PPFD activity factor (γ_P) has lower influence.

4.1.3 Evaluation of trace gas compounds

About 3000 air quality monitoring stations of 34 countries across Europe were analyzed from the AirBase database (https://www.eea.europa.eu/data-and-maps/data/aqereporting-8) for O_3, and its precursors (i.e., CO, and NO_2). Since discrepancies between modelled and measured values might be related to the type and location of a measurement station, the selected stations were also disaggregated into categories based on the study done by Henne et al., 2010, which includes a more complete analysis of the surroundings of each station. The alternative classification provides three class station types: urban, suburban and rural surface stations. Urban means a continuously built-up urban area (buildings with at least two floors), and the built-up area is not mixed with non-urbanized areas; suburban area is largely built-up urban area, with contiguous settlement of detached buildings of any size and the built-up area mixed with non-urbanized areas (e.g., agricultural, lakes, and woods). All areas, that do not achieve the criteria for urban or suburban areas, are defined as rural areas.

For each station the weekly mean of the concentrations was calculated for the daytime hours, from 7:00 am to 18:00 pm UTC. The mean bias, the normalized root means square error, and the correlation coefficient were calculated between the measured and simulated compounds (i.e., O_3, NO_2, and CO) for the different station classes (i.e., urban, suburban, and rural stations). Regardless of the monitoring stations type (i.e., urban, suburban, and rural), the M2.10, MG, and MGPFT runs show similar

statistics for ozone, with a consistent overestimation of its concentrations compared to the M2.04. For each model run and type of station, comparison between modelled and measured ozone concentrations shows positive mean bias values in the range 15–41% (Table 5). The ozone concentrations in rural areas present the lowest biases (M2.04 = 15 %, MG = MGPFT = 24 % and M2.10 = 23 %), while the highest biases are from the urban scenario (M2.04 = 31 %, M2.10 = 40 % and MG = MGPFT = 41 %). The MEGAN updates increase the mean biases of ozone concentrations by about 10 % regardless of the type of station considered. The changes to the MEGAN algorithm (i.e., MG, MGPFT, and M2.10 runs) have a small to negligible effect on modelled NO_2 and CO, with only CO having an increase of 2–4 % from the control simulation M2.04 compared to the other model runs (Table 5).

For the different model runs anthropogenic, biogenic and biomass burning NO_x emissions did not vary. Specifically, soil NO_x emissions were evaluated with MEGAN as a function of environment variables (i.e., temperature and vegetation types) that were the same for each model run. Therefore, no substantial changes were noted for the NO_x concentration levels for the different model runs. Recent studies regarding the effects of NO_x soil emissions on O_3 levels in California (USA) (Sha et al., 2021) and Europe (Visser et al., 2019) have pointed out that NO_x levels were underestimated with large biases because of the low NO_x soil emissions estimated with WRF-Chem/MEGAN. NO_x soil emissions are important both on the tropospheric NO_x budget and surface O_3 level perspectives (Sha et al., 2021). Considering that the model runs with increases in BVOC emissions showed higher O_3 levels, it is likely that the O_3 formation was not NO_x limited. MEGAN estimates carbon monoxide emissions as biogenic emission class unlike NO_x soil emissions. Higher CO emissions were noted for the MG simulation compared to the control run (M2.04) because of the changes in emission activity factors (γ_i). As reported in Table 2, CO emission factor differs between MG and MGPFT runs, with a lower value for MGPFT (600 CO μg m^{-2} hr^{-1}) compared to MG (1000 CO μg m^{-2} hr^{-1}). Moreover, the higher emission activity factor and lower CO emission factor in MGPFT compared to the control run resulted in only slight differences in CO levels between the two runs. Therefore, the different model runs showing slight variations in CO levels.

Since changes to NO_2 and CO emissions and mixing ratios were small, the increase in the O_3 biases may be due to the increased biogenic VOC emissions. Formaldehyde (HCHO), which is a product of BVOC chemistry, can play an important role in O_3 formation. The HCHO to NO_2 ratio is often used to show the role of VOCs on O_3 production, where higher HCHO to NO_2 ratios indicate higher O_3 production (e.g., Souri et al., 2020). A comparison of HCHO to NO_2 ratios for M2.04 and M2.10 simulations (Figure 13) show that in general HCHO/NO_2 is higher in the M2.10 simulation than the M2.04 simulation, suggesting that the higher BVOC emissions promoted more HCHO formation and subsequently O_3 formation.

There are strong positive correlations between modelled and observed O_3 concentrations, with slightly higher values of the correlation coefficient for MG, MGPFT, and M2.10 compared to M2.04. The ozone correlation coefficients are higher for the rural monitoring stations ($O_{3\text{-rural}}$ = 0.84-0.86), followed by the urban and suburban stations with values of about 0.75. Comparisons between modelled and measured ozone concentrations at rural background monitoring stations limit the influence of the model resolution (Table 5) (Jiang et al., 2019). Table 5 presents nitrogen dioxide correlation coefficient values in the range of 0.22–0.43, again with the lowest values for the urban and suburban stations and, the correlation coefficients for CO,

with low values (-0.02 to 0.22) for all the types of monitoring stations. There are no remarkable modifications with the different MEGAN updates simulations: O_3 and CO have an increase of about 0.01–0.02 from the control run (M2.04) to the MEGAN updates simulations (MG, MGPFT, and M2.10), while nitrogen dioxide correlation coefficient has literally no variations between the different MEGAN updates. Figure 16 displays scatter plots and regression lines having on the ordinate axis the observed (AirBase dataset) concentrations, and on the abscissa axis, the simulations performed (i.e., M2.04 and M2.10 runs). The concentrations of O_3, NO_2, and CO observed and modelled support the statistical analysis of biases, RMSEs, and correlation coefficients.

To learn how the spatial variation compares between observed and predicted trace gases, maps of mean day time (7 am – 6 pm UTC) concentrations of O_3, CO, and NO_2 (Figure 17) are examined for both the M2.04 control simulation and the M2.10 run with all the MEGAN code updates included. The spatial distribution of modelled ozone concentrations depicts well the observed values. However, the overestimation of the O_3 concentrations compared to the Airbase data is about 20 μg m^{-3} (about 10 ppb) and up to about 40 μg m^{-3} (about 20 ppb) for the M2.04 and M2.10 simulations, respectively. The overestimation is visible for most of Europe irrespective of the measured levels of O_3 concentration, but it is more evident in central Europe (France, Germany, Switzerland, Austria and Northern Italy) and the south coast of the Iberian Peninsula. The results here contrast with those by Jiang et al. (2019), who found modelled ozone using the BVOC emission input from MEGAN v2.1 to be overestimated at low mixing ratios (20–50 ppb) and generally underestimated at mixing ratios above 50 ppb irrespective of the region of Europe considered. The NO_2 (Figure 17-b) concentration spatial distribution is not well represented by WRF-Chem, especially in north Europe (i.e., England, Belgium, Netherlands and North Germany), Northern Italy and Northeastern Spain. There is a large underestimation of NO_2 by the model in central Europe, where the difference is a factor of 10 (from 5 to 50 μg m^{-3} - approximately from 2.5 to 5 ppb). This may be due to the lack of updated anthropogenic emissions as the EDGAR-HTAP emissions (Janssens-Maenhout et al., 2012) represent 2010 not 2015 which impacts the nitrogen oxides that are mainly emitted from anthropogenic sources (e.g. road traffic), or due to the 12-km grid spacing in WRF-Chem not resolving high concentrations in urban locations.

The WRF-Chem model underestimates CO concentrations by a factor of 2 (from 240 to 500 μg m^{-3} - approximately from 210 to 435 ppb) for most of the stations measured (Figure 17-c), with the measured CO spatial distribution having no definite geographic pattern. The difference between measured and modelled CO concentrations is more evident across Italy, the south of Spain, Poland, and Czech Republic. The magnitude of the gap in Eastern Europe could be a sign the model biomass burning emissions (FINN emissions - Wiedinmyer *et al.*, 2011) could not represent well the overview of the situation. Figure S6 shows a comparison between weekly average CO concentrations evaluated with the M2.10 run (Figure S6-a), and a simulation with the same model setup with no biomass burning emissions (Figure S6-b - "M2.10_noFINN"). The difference between the two simulations is clear in Eastern Europe, without including the biomass burning emissions the CO concentration decreases from 240-320 to 160-240 μg m^{-3} interval (209-280 to 140-209 ppb). This indicates a presence of wildfire in that area, captured by both the Airbase dataset and the model, but not sufficiently represented by biomass burning emissions and their computation in WRF-Chem. NO_2 concentrations are also affected by the biomass burning emissions (Figure S7) but not as strongly as the

CO concentrations. In general, the NO_2 differences between the M2.10 run (Figure S7-a) and the simulations with no biomass burning emissions (Figure S7-b - "M2.10_noFINN") are about 5 ug m^{-3}. Moreover, both the CO and NO_2 concentrations do not show differences in spatial resolution and concentration magnitude between the MEGAN update simulations (Figure 17).

4.2 Southeast US Case Study

Since the Southeast US Case Study encompasses the NOMADSS field campaign, simulated biogenic VOCs and other trace gases can be evaluated. The MEGAN code updates are compared with the NOMADSS NCAR C-130 flight measurements to investigate the ability of the M2.04 and M2.10 simulations in depicting the BVOC composition in the boundary layer.

4.2.1 Evaluation of trace gas compounds

Figure 18 shows the altitude of the flight, the temperature, the mixing ratios of isoprene, methacrolein (MACR), methyl vinyl ketone (MVK), and ozone measured during the June 5th, 2013 (14 - 21 UTC; 9 - 16 US central daylight time) flight (Figure 18). Similar figures for flights on June 3rd, 8th, 12th, and 14th are shown in Figures S8 to S11. Isoprene, MACR, and MVK were measured by The Trace Organic Gas Analyzer (TOGA), which is a fast online Gas Chromatograph/Mass Spectrometer (GC/MS), with a measurement frequency of approximately one 30s sample every 2 minutes (Apel et al., 2003). Uncertainties of isoprene, MACR, and MVK are reported to be 15%, 20%, and 20% of the measured mixing ratio, respectively.

To explore the PBL ozone evolution, we examine the June 5th flight measurements since these measurements have a clear time frame (Figure 18- a) (i.e., from 16:15 – 18:45 UTC time or 11:15 – 13:45 US central daylight time) when the aircraft was lower than the PBL height as it was flying near the Texas-Louisiana border (Figure 3). Comparison of M2.04 and M2.10 simulations to aircraft observations shows that isoprene (Figure 18-c) mixing ratios agree well with measured isoprene for the M2.04 simulation but are overpredicted by up to 10 ppbv in the PBL. In response, MACR (Figure 18-d), a product of isoprene (Table S2 in the supplement materials), is also overpredicted by the M2.10 simulation by up to a factor of 4, while MACR is either well-predicted or overestimated by up to a factor of 2 by the M2.04 simulation. MVK (Figure 18-e), an isoprene-dependent compound, has the opposite trend. That is, MVK flight track measurements are more similar to the M2.10 run than the M2.04 simulation. In response to the higher isoprene, ozone mixing ratios (Figure 18-f) are affected with MEGAN v2.04 results showing more similarity to measurements than the M2.10 simulation, which generally overpredicts ozone by 10-20 ppbv. Table S3 shows a statistical analysis of the model-observation normalized root mean square errors, correlations, and biases. Like shown in the figures, the inclusion of updates from M2.04 to M2.10 tends to worsen the agreement with observations.

Often, CTMs tend to significantly overestimate surface ozone in the U.S. (Brown-Steiner et al., 2015; Fiore et al., 2009; Lin et al., 2008). Recent studies have shed a light on modelling surface ozone in the southeast U.S. (Travis et al., 2016; Schwantes et al., 2020; Cuchiara et al., 2020). Travis et al. (2016) investigated the main driving factors for the overestimation of modelled surface O_3 concentrations in the Southeast U.S. comparing CTM (i.e, Geos-Chem) predictions with multiplatform observations. These authors observed that a correction to the high-biased NO_x emissions led to better matching modelled and

measured O_3 concentrations both in the PBL and in the free troposphere. Cuchiara et al. (2020) have investigated the interactions between cloud microphysics and the convective transport of soluble O_3 precursors from PBL to the upper troposphere. These authors applied a 50 % reduction to the biogenic isoprene emission calculated with MEGAN v2.04 for WRF-Chem 3.9.1 based on the bias observed by previous studies in the U.S. southeast. A comprehensive study by Schwantes et al. (2020) dealt with a more detailed description of isoprene and terpene chemistry for modelling surface ozone with CAM-chem during the summer 2013 time period. Based on sensitivity tests, Schwantes et al. (2020) observed that the more detailed isoprene chemistry representation improved agreement with the surface ozone daily max 8 h average values. Further, a paper by Ryu et al. 2018 clarifies the effect of cloud prediction on ozone: having clouds in the right place at the right time also improved ozone predictions. Nevertheless, for our study this is likely not the cause, and the ozone overprediction is mainly due to the isoprene emission changes. According to large-eddy simulations (Kim et al., 2016; Li et al., 2016; Ouwersloot et al., 2011) and measurement-model analysis (Kaser et al., 2015) the effects of physical separation of isoprene and OH in the PBL depends on chemistry-turbulence interactions and scale dependent heterogeneity of isoprene emissions, with potential implications on CTMs. The differences observed between measured and modelled isoprene mixing ratios along flight tracks may depend on the complex interaction between chemical reactions involving isoprene and turbulence within the PBL (Zhao et al., 2016). However, aircraft measurements generally take place under weather conditions and boundary layer heights scarcely affected by boundary layer mixing phenomena (Travis et al., 2016).Therefore, differences between modelled and aircraft data, that were observed in the present study, likely do not depend on simulated values of boundary layer meteorological variables.

5. Conclusions

To compare different updates to MEGAN v2.04 introduced by G12 with MEGAN v2.1 in simulating biogenic volatile organic compound (BVOC) emissions, two case studies were performed in two different domains (i.e., Europe and the Southeast United States). A sensitivity study on BVOC emissions was performed for a high-ozone episode in August 2015 in Europe considering a control run with MEGAN v.2.04 (i.e., M2.04) and the (i) update of the emission activity factors (i.e., MG), (ii) update of the emission factor values for each plant functional type (PFT) (i.e., MGPFT), and (iii) the assignment of the emission factor by PFT to isoprene (i.e., M2.10).

Comparisons between modelled and surface measured (Airbase database) ozone concentrations showed values of the correlation coefficients in the range from 0.78 to 0.86, with higher values for the rural monitoring stations compared to the urban and suburban ones. Correlation coefficients were higher in the M2.10 run compared to the M2.04 simulation. Moreover, the spatial distribution of modelled O_3 concentrations represented well the observed values, regardless of the simulations considered (M2.04, MG, MGPFT, and M2.10). However, magnitude differences were observed in both M2.04 and M2.10 simulations, with an overestimation of the O_3 concentrations compared to the Airbase data by about 20 $\mu g\ m^{-3}$ (10 ppb) and up to about 40 $\mu g\ m^{-3}$ (20 ppb), respectively.

For the Southeast United States case study, modelled BVOC emissions were evaluated against aircraft measurements to investigate the performance of M2.04 and M2.10 runs in depicting the BVOC dynamics in the planetary boundary layer (PBL). The measurements of isoprene, two products of isoprene oxidation (i.e., methacrolein, and methyl vinyl ketone) and ozone were taken in five of the research flights under the Southern Oxidant and Aerosol Study in June 2013. To analyze the PBL ozone evolution, flight measurements were considered when the flight track height was lower than the PBL height showed that the M2.04 simulation better represented the flight track isoprene mixing ratios than the M2.10 simulation. Each of the five research flights examined showed a M2.10 overestimation of isoprene mixing ratios up to a factor of 5. Comparisons between measured and modelled methacrolein and ozone reflected the isoprene comparison, with M2.04 results more similar to flight track measurements than the updated M2.10 simulation. Methyl vinyl ketone showed an opposite trend to the isoprene one, with the M2.10 results more like the flight track measurements than the control simulation.

In summary, the MEGAN updates (M2.10) generate substantially higher emissions of BVOCs, by factors of two or more. For both situations modelled here, better agreement with observations is obtained using the older emissions (M2.04). Mainly, the simulations with updated emissions incurred larger biases in ozone measured across Europe, and overpredicted the concentrations of BVOC and their oxidation products observed directly during aircraft flights in the south-eastern US. Both comparisons showed that BVOC emissions are better represented in M2.04 than in M2.10, suggesting further improvements are needed. These improvements should include increasing the number of PFTs from four, used in this study, to 15, used in G12, and adding effects of the canopy and stress factors (Zhang et al., 2021), which are part of MEGAN v3. We also suggest further tests at different grid spacing so that vegetation variability and emission factors can be assessed. While we note substantial differences between M2.04 and M2.10 simulations, other factors in the WRF-Chem simulations could have affected the model evaluation. These other factors include underestimations of CO and NO_2 affecting the comparison with O_3 over Europe. Accurate anthropogenic and biomass-burning emissions are also necessary for future evaluation. Cloudiness not only can directly affect biogenic emissions, but also photolysis rates, which impacts the ozone production (e.g., Ryu et al., 2018). Evaluation of the chemistry can also be aided by comparing WRF-Chem model results with satellite observations. For example, formaldehyde satellite measurements have been used to infer isoprene emissions (Curci et al., 2010). We lastly advocate for continued field measurements to refine emission factors with various vegetation types across the globe and experiments to better characterize the emission activity factors.

Code availability. The WRF-Chem code is available at http://www2.mmm.ucar.edu/wrf/users/download/get_source.html. The code of updated MEGAN version (WRF-Chem modules: module_bioemi_megan2.F and module_data_megan2.F) can be obtained from Mauro Morichetti (m.morichetti@isac.cnr.it).

Author contributions. The first author (MM) developed and implemented the updates, performed the simulations and the analysis, and drafted the paper. MB contributed to simulation design, to the interpretation of results, and to writing the paper. SM contributed to conceptualizing the paper. GP contributed to funding acquisition. EM and SV helped to review and editing the paper. UR supervised the entire writing-editing paper process.

Competing interests. The authors declare that they have no conflict of interest

Acknowledgments. Mauro Morichetti acknowledges funding from NCAR's Advanced Study Program's Graduate Student (GVP) fellowship. We would like to acknowledge high-performance computing support from Cheyenne (doi:10.5065/D6RX99HX) provided by NCAR's Computational and Information Systems Laboratory, sponsored by the National Science Foundation. We also acknowledge use of the WRF-Chem preprocessor tool (mozbc, fire_emiss, megan_emission and antro_emission) provided by the Atmospheric Chemistry Observations and Modeling Lab (ACOM) of NCAR. We greatly appreciate the contributions from Christine Wiedinmeyer in providing advice in conducting the project. We greatly appreciate the colleagues who obtained the measurements used in the paper. For the NOMADSS aircraft data, we acknowledge the NCAR-EOL-RAF team for state parameter data, A. Weinheimer, D. Knapp, D. Montzka, F. Flocke, and T. Campos for the ozone measurements, and E. Apel and R. Hornbrook for the volatile organic compounds data.

References

Andreani-aksoyoglu, S. and Keller, J.: Estimates of monoterpene and isoprene emissions from the forests in Switzerland, J. Atmos. Chem., 20(1), 71–87, doi:10.1007/BF01099919, 1995.

Apel, E. C., Hills, A. J., Lueb, R., Zindel, S., Eisele, S. and Riemer, D. D.: A fast-GC-MS system to measure C2 to C4 carbonyls and methanol aboard aircraft, J. Geophys. Res. Atmos., 108(20), 8794, doi:10.1029/2002jd003199, 2003.

Arneth, A., Niinemets, Ü., Pressley, S., Bäck, J., Hari, P., Karl, T., Noe, S., Prentice, I. C., Serça, D., Hickler, T., Wolf, A. and Smith, B.: Process-based estimates of terrestrial ecosystem isoprene emissions: incorporating the effects of a direct CO₂-isoprene interaction, Atmos. Chem. Phys., 7(1), 31–53, doi:10.5194/acp-7-31-2007, 2007.

Bey, I., Jacob, D. J., Yantosca, R. M., Logan, J. A., Field, B. D., Fiore, A. M., Li, Q., Liu, H. Y., Mickley, L. J. and Schultz, M. G.: Global modeling of tropospheric chemistry with assimilated meteorology: Model description and evaluation, J. Geophys. Res. Atmos., 106(D19), 23073–23095, doi:10.1029/2001JD000807, 2001.

Brasseur, G. P., Kiehl, J. T., Müller, J. F., Schneider, T., Granier, C., Tie, X. X. and Hauglustaine, D.: Past and future changes in global tropospheric ozone: Impact on radiative forcing, Geophys. Res. Lett., 25(20), 3807–3810, doi:10.1029/1998GL900013, 1998.

Brown-Steiner, B., Hess, P. G. and Lin, M. Y.: On the capabilities and limitations of GCCM simulations of summertime regional air quality: A diagnostic analysis of ozone and temperature simulations in the US using CESM CAM-Chem, Atmos. Environ., 101, 134–148, doi:10.1016/j.atmosenv.2014.11.001, 2015.

Carlton, A. G., de Gouw, J., Jimenez, J., Ambrose, J., Attwood, A., Brown, S., BAKer, K., BroCK, C., Cohen, ronAld C., EdGerton, S., FArKAs, Ca., FArmer, D., Goldstein, A., GrAtz, L., Guenther, A., Hunt, S., JAeGlé, L., JAFFe, dAniel A., MAK, J., MCClure, C., Stutz, J., SurrAtt, Ja., Turpin, bArbArA J., WArneKe, Ca., WAshenFelder, rebeCCA A., WennberG, Pa. and Zhou, xiAnlinG T.: United Nations (UN; IRAC 2013), and Intergovernmental Panel on Climate Change (IPCC), , doi:10.1175/BAMS-D-16-0048.1, 2014.

Chen, F. and Dudhia, J.: Coupling an Advanced Land Surface–Hydrology Model with the Penn State–NCAR MM5 Modeling System. Part I: Model Implementation and Sensitivity, Mon. Weather Rev., 129(4), 569–585, doi:10.1175/1520-0493(2001)129<0569:CAALSH>2.0.CO;2, 2001.

Chen, F., Mitchell, K., Schaake, J., Xue, Y., Pan, H.-L., Koren, V., Duan, Q. Y., Ek, M. and Betts, A.: Modeling of land surface evaporation by four schemes and comparison with FIFE observations, J. Geophys. Res. Atmos., 101(D3), 7251–7268, doi:10.1029/95JD02165, 1996.

Churkina, G., Kuik, F., Bonn, B., Lauer, A., Grote, R., Tomiak, K. and Butler, T. M.: Effect of VOC Emissions from Vegetation on Air Quality in Berlin during a Heatwave, Environ. Sci. Technol., 51(11), 6120–6130, doi:10.1021/acs.est.6b06514, 2017.

Cuchiara, G. C., Fried, A., Barth, M. C., Bela, M., Homeyer, C. R., Gaubert, B., Walega, J., Weibring, P., Richter, D., Wennberg, P., Crounse, J., Kim, M., Diskin, G., Hanisco, T. F., Wolfe, G. M., Beyersdorf, A., Peischl, J., Pollack, I. B., St. Clair, J. M., Woods, S., Tanelli, S., Bui, T. V., Dean-Day, J., Huey, L. G. and Heath, N.: Vertical Transport, Entrainment, and Scavenging Processes Affecting Trace Gases in a Modeled and Observed SEAC4RS Case Study, J. Geophys. Res. Atmos., 125(11), e2019JD031957, doi:10.1029/2019JD031957, 2020.

Curci, G., Palmer, P. I., Kurosu, T. P., Chance, K. and Visconti, G.: Estimating European volatile organic compound emissions using satellite observations of formaldehyde from the Ozone Monitoring Instrument, Atmos. Chem. Phys., 10(23), 11501–11517, doi:10.5194/acp-10-11501-2010, 2010.

van Donkelaar, A., Martin, R. V., Park, R. J., Heald, C. L., Fu, T.-M., Liao, H. and Guenther, A.: Model evidence for a significant source of secondary organic aerosol from isoprene, Atmos. Environ., 41(6), 1267–1274, doi:10.1016/J.ATMOSENV.2006.09.051, 2007.

EEA: Air pollution due to ozone: health impacts and effects of climate change, 2015.

EEA: Air Quality in Europe 2017 Report, Luxembourg., 2017.

Emmons, L. K., Walters, S., Hess, P. G., Lamarque, J. F., Pfister, G. G., Fillmore, D., Granier, C., Guenther, A., Kinnison, D., Laepple, T., Orlando, J., Tie, X., Tyndall, G., Wiedinmyer, C., Baughcum, S. L. and Kloster, S.: Description and evaluation of the Model for Ozone and Related chemical Tracers, version 4 (MOZART-4), Geosci. Model Dev., 3(1), 43–67, doi:10.5194/gmd-3-43-2010, 2010.

Fast, J. D., Gustafson, W. I., Easter, R. C., Zaveri, R. A., Barnard, J. C., Chapman, E. G., Grell, G. A. and Peckham, S. E.: Evolution of ozone, particulates, and aerosol direct radiative forcing in the vicinity of Houston using a fully coupled meteorology-chemistry-aerosol model, J. Geophys. Res. Atmos., 111(21), D21305, doi:10.1029/2005JD006721, 2006.

Fehsenfeld, F., Calvert, J., Fall, R., Goldan, P., Guenther, A. B., Hewitt, C. N., Lamb, B., Liu, S., Trainer, M., Westberg, H. and Zimmerman, P.: Emissions of volatile organic compounds from vegetation and the implications for atmospheric chemistry, Global Biogeochem. Cycles, 6(4), 389–430, doi:10.1029/92GB02125, 1992.

Fiore, A. M., Dentener, F. J., Wild, O., Cuvelier, C., Schultz, M. G., Hess, P., Textor, C., Schulz, M., Doherty, R. M., Horowitz, L. W., MacKenzie, I. A., Sanderson, M. G., Shindell, D. T., Stevenson, D. S., Szopa, S., Van Dingenen, R., Zeng, G., Atherton, C., Bergmann, D., Bey, I., Carmichael, G., Collins, W. J., Duncan, B. N., Faluvegi, G., Folberth, G., Gauss, M., Gong, S., Hauglustaine, D., Holloway, T., Isaksen, I. S. A., Jacob, D. J., Jonson, J. E., Kaminski, J. W., Keating, T. J., Lupu, A., Manner, E., Montanaro, V., Park, R. J., Pitari, G., Pringle, K. J., Pyle, J. A., Schroeder, S., Vivanco, M. G., Wind, P., Wojcik, G., Wu, S. and Zuber, A.: Multimodel estimates of intercontinental source-receptor relationships for ozone pollution, J. Geophys. Res.

Atmos., 114(4), D04301, doi:10.1029/2008JD010816, 2009.

Gauss, M., Myhre, G., Isaksen, I. S. A., Grewe, V., Pitari, G., Wild, O., Collins, W. J., Dentener, F. J., Ellingsen, K., Gohar, L. K., Hauglustaine, D. A., Iachetti, D., Lamarque, F., Mancini, E., Mickley, L. J., Prather, M. J., Pyle, J. A., Sanderson, M. G., Shine, K. P., Stevenson, D. S., Sudo, K., Szopa, S. and Zeng, G.: Radiative forcing since preindustrial times due to ozone change in the troposphere and the lower stratosphere, Atmos. Chem. Phys., 6(3), 575–599, doi:10.5194/acp-6-575-2006, 2006.

Grell, G. A. and Freitas, S. R.: A scale and aerosol aware stochastic convective parameterization for weather and air quality modeling, Atmos. Chem. Phys., 14(10), 5233–5250, doi:10.5194/acp-14-5233-2014, 2014.

Grell, G. A., Peckham, S. E., Schmitz, R., McKeen, S. A., Frost, G., Skamarock, W. C. and Eder, B.: Fully coupled "online" chemistry within the WRF model, Atmos. Environ., 39(37), 6957–6975, doi:10.1016/j.atmosenv.2005.04.027, 2005.

Guenther, A., Hewitt, C. N., Erickson, D., Fall, R., Geron, C., Graedel, T., Harley, P., Klinger, L., Lerdau, M., Mckay, W. A., Pierce, T., Scholes, B., Steinbrecher, R., Tallamraju, R., Taylor, J. and Zimmerman, P.: A global model of natural volatile organic compound emissions, J. Geophys. Res., 100(D5), 8873, doi:10.1029/94JD02950, 1995.

Guenther, A., Baugh, B., Brasseur, G., Greenberg, J., Harley, P., Klinger, L., Serça, D. and Vierling, L.: Isoprene emission estimates and uncertainties for the central African EXPRESSO study domain, J. Geophys. Res. Atmos., 104(D23), 30625–30639, doi:10.1029/1999JD900391, 1999.

Guenther, A., Karl, T., Harley, P., Wiedinmyer, C., Palmer, P. I. and C., G.: Estimates of global terrestrial isoprene emissions using MEGAN, Atmos. Chem. Phys. Discuss., 6(1), 107–173, doi:10.5194/acpd-6-107-2006, 2006.

Guenther, A., Jiang, X., Heald, C. L., Sakulyanontvittaya, T., Duhl, T., Emmons, L. K. and Wang, X.: The model of emissions of gases and aerosols from nature version 2.1 (MEGAN2.1): An extended and updated framework for modeling biogenic emissions, Geosci. Model Dev., 5(6), 1471–1492, doi:10.5194/gmd-5-1471-2012, 2012.

Guenther, A., Jiang, X., Shah, T., Huang, L., Kemball-Cook, S. and Yarwood, G.: Model of Emissions of Gases and Aerosol from Nature Version 3 (MEGAN3) for Estimating Biogenic Emissions, in Springer Proceedings in Complexity, pp. 187–192, Springer, Cham., 2020.

Guenther, A. B., Zimmerman, P. R., Harley, P. C., Monson, R. K. and Fall, R.: Isoprene and monoterpene emission rate variability: Model evaluations and sensitivity analyses, J. Geophys. Res., 98(D7), 12609, doi:10.1029/93JD00527, 1993.

Henne, S., Brunner, D., Folini, D., Solberg, S., Klausen, J. and Buchmann, B.: Assessment of parameters describing representativeness of air quality in-situ measurement sites, Atmos. Chem. Phys., 10(8), 3561–3581, doi:10.5194/acp-10-3561-2010, 2010.

Henrot, A. J., Stanelle, T., Schröder, S., Siegenthaler, C., Taraborrelli, D. and Schultz, M. G.: Implementation of the MEGAN (v2.1) biogenic emission model in the ECHAM6-HAMMOZ chemistry climate model, Geosci. Model Dev., 10(2), 903–926, doi:10.5194/gmd-10-903-2017, 2017.

Iacono, M. J., Delamere, J. S., Mlawer, E. J., Shephard, M. W., Clough, S. A. and Collins, W. D.: Radiative forcing by long-lived greenhouse gases: Calculations with the AER radiative transfer models, J. Geophys. Res. Atmos., 113(13), D13103, doi:10.1029/2008JD009944, 2008.

Im, U., Markakis, K., Poupkou, A., Melas, D., Unal, A., Gerasopoulos, E., Daskalakis, N., Kindap, T. and Kanakidou, M.: The impact of temperature changes on summer time ozone and its precursors in the Eastern Mediterranean, Atmos. Chem. Phys., 11(8), 3847–3864, doi:10.5194/acp-11-3847-2011, 2011.

Im, U., Markakis, K., Koçak, M., Gerasopoulos, E., Daskalakis, N., Mihalopoulos, N., Poupkou, A., Kındap, T., Unal, A. and Kanakidou, M.: Summertime aerosol chemical composition in the Eastern Mediterranean and its sensitivity to temperature, Atmos. Environ., 50, 164–173, doi:10.1016/J.ATMOSENV.2011.12.044, 2012.

Ionita, M., Tallaksen, L. M., Kingston, D. G., Stagge, J. H., Laaha, G., Van Lanen, H. A. J., Scholz, P., Chelcea, S. M. and Haslinger, K.: The European 2015 drought from a climatological perspective, Hydrol. Earth Syst. Sci., 21(3), 1397–1419, doi:10.5194/hess-21-1397-2017, 2017.

Janjić, Z. I.: The Step-Mountain Eta Coordinate Model: Further Developments of the Convection, Viscous Sublayer, and Turbulence Closure Schemes, Mon. Weather Rev., 122(5), 927–945, doi:10.1175/1520-0493(1994)122<0927:TSMECM>2.0.CO;2, 1994.

Janssens-Maenhout, G., Dentener, F., Van Aardenne, J., Monni, S., Pagliari, V., Orlandini, L., Klimont, Z., Kurokawa, J., Akimoto, H., Ohara, T., Wankmueller, R., Battye, B., Grano, D., Zuber, A. and Keating, T.: EDGAR-HTAP: a Harmonized Gridded Air Pollution Emission Dataset Based on National Inventories, Ispra (Italy): European Commission Publications Office., 2012.

Jiang, J., Aksoyoglu, S., Ciarelli, G., Oikonomakis, E., El-Haddad, I., Canonaco, F., O'dowd, C., Ovadnevaite, J., Minguillón, M. C., Baltensperger, U. and Cruz, M.: Effects of two different biogenic emission models on modelled ozone and aerosol concentrations in Europe, Atmos. Chem. Phys., 19(6), 3747–3768, doi:10.5194/acp-19-3747-2019, 2019.

Jiang, X., Guenther, A., Potosnak, M., Geron, C., Seco, R., Karl, T., Kim, S., Gu, L. and Pallardy, S.: Isoprene emission response to drought and the impact on global atmospheric chemistry, Atmos. Environ., 183(January), 69–83, doi:10.1016/j.atmosenv.2018.01.026, 2018.

Kaser, L., Karl, T., Yuan, B., Mauldin, R. L., Cantrell, C. A., Guenther, A. B., Patton, E. G., Weinheimer, A. J., Knote, C., Orlando, J., Emmons, L., Apel, E., Hornbrook, R., Shertz, S., Ullmann, K., Hall, S., Graus, M., De Gouw, J., Zhou, X. and Ye, C.: Chemistry-turbulence interactions and mesoscale variability influence the cleansing efficiency of the atmosphere, Geophys. Res. Lett., 42(24), 10894–10903, doi:10.1002/2015GL066641, 2015.

Keenan, T., Niinemets, Ü., Sabate, S., Gracia, C. and Peñuelas, J.: Process based inventory of isoprenoid emissions from European forests: Model comparisons, current knowledge and uncertainties, Atmos. Chem. Phys., 9(12), 4053–4076, doi:10.5194/acp-9-4053-2009, 2009.

Kim, S.-W., Barth, M. C. and Trainer, M.: Impact of turbulent mixing on isoprene chemistry, Geophys. Res. Lett., 43(14), 7701–7708, doi:10.1002/2016GL069752, 2016.

Lamarque, J. F., Emmons, L. K., Hess, P. G., Kinnison, D. E., Tilmes, S., Vitt, F., Heald, C. L., Holland, E. A., Lauritzen, P. H., Neu, J., Orlando, J. J., Rasch, P. J. and Tyndall, G. K.: CAM-chem: Description and evaluation of interactive atmospheric chemistry in the Community Earth System Model, Geosci. Model Dev., 5(2), 369–411, doi:10.5194/gmd-5-369-2012, 2012.

Lawrence, D. M., Oleson, K. W., Flanner, M. G., Thornton, P. E., Swenson, S. C., Lawrence, P. J., Zeng, X., Yang, Z.-L., Levis, S., Sakaguchi, K., Bonan, G. B. and Slater, A. G.: Parameterization improvements and functional and structural advances in Version 4 of the Community Land Model, J. Adv. Model. Earth Syst., 3(3), doi:10.1029/2011ms000045, 2011.

Li, Y., Barth, M. C., Chen, G., Patton, E. G., Kim, S.-W., Wisthaler, A., Mikoviny, T., Fried, A., Clark, R. and Steiner, A. L.: Large-eddy simulation of biogenic VOC chemistry during the DISCOVER-AQ 2011 campaign, J. Geophys. Res. Atmos., 121(13), 8083–8105, doi:10.1002/2016JD024942, 2016.

Limbeck, A., Kulmala, M. and Puxbaum, H.: Secondary organic aerosol formation in the atmosphere via heterogeneous reaction of gaseous isoprene on acidic particles, Geophys. Res. Lett., 30(19), 1996, doi:10.1029/2003GL017738, 2003.

Lin, J. T., Youn, D., Liang, X. Z. and Wuebbles, D. J.: Global model simulation of summertime U.S. ozone diurnal cycle and its sensitivity to PBL mixing, spatial resolution, and emissions, Atmos. Environ., 42(36), 8470–8483, doi:10.1016/j.atmosenv.2008.08.012, 2008.

Lin, M., Horowitz, L. W., Xie, Y., Paulot, F., Malyshev, S., Shevliakova, E., Finco, A., Gerosa, G., Kubistin, D. and Pilegaard, K.: Vegetation feedbacks during drought exacerbate ozone air pollution extremes in Europe, Nat. Clim. Chang., 10(5), 444–451, doi:10.1038/s41558-020-0743-y, 2020.

Martin, M. J., Stirling, C. M., Humphries, S. W. and Long, S. P.: A process-based model to predict the effects of climatic change on leaf isoprene emission rates, Ecol. Modell., 131(2–3), 161–174, doi:10.1016/S0304-3800(00)00258-1, 2000.

Messina, P., Lathière, J., Sindelarova, K., Vuichard, N., Granier, C., Ghattas, J., Cozic, A. and Hauglustaine, D. A.: Global biogenic volatile organic compound emissions in the ORCHIDEE and MEGAN models and sensitivity to key parameters, Atmos. Chem. Phys., 16(22), 14169–14202, doi:10.5194/acp-16-14169-2016, 2016.

Morrison, H., Thompson, G. and Tatarskii, V.: Impact of Cloud Microphysics on the Development of Trailing Stratiform Precipitation in a Simulated Squall Line: Comparison of One- and Two-Moment Schemes, Mon. Weather Rev., 137(3), 991–1007, doi:10.1175/2008MWR2556.1, 2009.

National Centers for Environmental Prediction - National Weather Service NOAA U. S. Department of Commerce: NCEP North American Regional Reanalysis (NARR), [online] Available from: https://rda.ucar.edu/datasets/ds608.0/ (Accessed 25 November 2018), 2005.

Ncep: NCEP FNL Operational Model Global Tropospheric Analyses, continuing from July 1999, Dataset ds083. 2 Publ. by CISL Data Support …, doi:10.5065/D6M043C6, 2000.

Niinemets, U., Tenhunen, J. D., Harley, P. C. and Steinbrecher, R.: A model of isoprene emission based on energetic requirements for isoprene synthesis and leaf photosynthetic properties for Liquidambar and Quercus, Plant, Cell Environ., 22(11), 1319–1335, doi:10.1046/j.1365-3040.1999.00505.x, 1999.

Niu, G. Y., Yang, Z. L., Mitchell, K. E., Chen, F., Ek, M. B., Barlage, M., Kumar, A., Manning, K., Niyogi, D., Rosero, E., Tewari, M. and Xia, Y.: The community Noah land surface model with multiparameterization options (Noah-MP): 1. Model description and evaluation with local-scale measurements, J. Geophys. Res. Atmos., 116(12), D12109, doi:10.1029/2010JD015139, 2011.

Oleson, W., Lawrence, M., Bonan, B., Flanner, G., Kluzek, E., Lawrence, J., Levis, S., Swenson, C., Thornton, E., Dai, A., Decker, M., Dickinson, R., Feddema, J., Heald, L., Hoffman, F., Lamarque, J.-F., Mahowald, N., Niu, G.-Y., Qian, T., Randerson, J., Running, S., Sakaguchi, K., Slater, A., Stockli, R., Wang, A., Yang, Z.-L., Zeng, X. and Zeng, X.: Technical Description of version 4.0 of the Community Land Model (CLM), , doi:10.5065/D6FB50WZ, 2010.

Ouwersloot, H. G., Vilà-Guerau de Arellano, J., van Heerwaarden, C. C., Ganzeveld, L. N., Krol, M. C. and Lelieveld, J.: On the segregation of chemical species in a clear boundary layer over heterogeneous land surfaces, Atmos. Chem. Phys., 11(20), 10681–10704, doi:10.5194/acp-11-10681-2011, 2011.

Pegoraro, E., Rey, A., Bobich, E. G., Barron-Gafford, G., Grieve, K. A., Malhi, Y. and Murthy, R.: Effect of elevated CO2 concentration and vapour pressure deficit on isoprene emission from leaves of Populus deltoides during drought, Funct. Plant Biol., 31(12), 1137–1147, doi:10.1071/FP04142, 2004.

Ryu, Y. H., Hodzic, A., Barre, J., Descombes, G. and Minnis, P.: Quantifying errors in surface ozone predictions associated with clouds over the CONUS: A WRF-Chem modeling study using satellite cloud retrievals, Atmos. Chem. Phys., 18(10), 7509–7525, doi:10.5194/acp-18-7509-2018, 2018.

Sakulyanontvittaya, T., Duhl, T., Wiedinmyer, C., Helmig, D., Matsunaga, S., Potosnak, M., Milford, J. and Guenther, A.: Monoterpene and sesquiterpene emission estimates for the United States, Environ. Sci. Technol., 42(5), 1623–1629, doi:10.1021/es702274e, 2008.

Sartelet, K. N., Couvidat, F., Seigneur, C. and Roustan, Y.: Impact of biogenic emissions on air quality over Europe and North America, Atmos. Environ., 53, 131–141, doi:10.1016/j.atmosenv.2011.10.046, 2012.

Schwantes, R. H., Emmons, L. K., Orlando, J. J., Barth, M. C., Tyndall, G. S., Hall, S. R., Ullmann, K., St. Clair, J. M., Blake, D. R., Wisthaler, A. and Paul V. Bui, T.: Comprehensive isoprene and terpene gas-phase chemistry improves simulated surface ozone in the southeastern US, Atmos. Chem. Phys., 20(6), 3739–3776, doi:10.5194/acp-20-3739-2020, 2020.

Sha, T., Ma, X., Zhang, H., Janechek, N., Wang, Y., Wang, Y., Castro García, L., Jenerette, G. D. and Wang, J.: Impacts of Soil NOxEmission on O3Air Quality in Rural California, Environ. Sci. Technol., 55(10), 7113–7122, doi:10.1021/acs.est.0c06834, 2021.

Sindelarova, K., Granier, C., Bouarar, I., Guenther, A., Tilmes, S., Stavrakou, T., Müller, J. F., Kuhn, U., Stefani, P. and Knorr, W.: Global data set of biogenic VOC emissions calculated by the MEGAN model over the last 30 years, Atmos. Chem. Phys., 14(17), 9317–9341, doi:10.5194/acp-14-9317-2014, 2014.

Souri, A. H., Nowlan, C. R., Wolfe, G. M., Lamsal, L. N., Chan Miller, C. E., Abad, G. G., Janz, S. J., Fried, A., Blake, D. R., Weinheimer, A. J., Diskin, G. S., Liu, X. and Chance, K.: Revisiting the effectiveness of HCHO/NO2 ratios for inferring ozone sensitivity to its precursors using high resolution airborne remote sensing observations in a high ozone episode during the KORUS-AQ campaign, Atmos. Environ., 224, 117341, doi:10.1016/J.ATMOSENV.2020.117341, 2020.

Travis, K. R., Jacob, D. J., Fisher, J. A., Kim, P. S., Marais, E. A., Zhu, L., Yu, K., Miller, C. C., Yantosca, R. M., Sulprizio, M. P., Thompson, A. M., Wennberg, P. O., Crounse, J. D., St Clair, J. M., Cohen, R. C., Laughner, J. L., Dibb, J. E., Hall, S. R., Ullmann, K., Wolfe, G. M., Pollack, I. B., Peischl, J., Neuman, J. A. and Zhou, X.: Why do models overestimate surface

ozone in the Southeast United States?, Atmos. Chem. Phys., 16(21), 13561–13577, doi:10.5194/acp-16-13561-2016, 2016.

Visser, A. J., Folkert Boersma, K., Ganzeveld, L. N. and Krol, M. C.: European NOx emissions in WRF-Chem derived from OMI: Impacts on summertime surface ozone, Atmos. Chem. Phys., 19(18), 11821–11841, doi:10.5194/acp-19-11821-2019, 2019.

Wang, Y., Tan, X., Huang, L., Wang, Q., Li, H., Zhang, H., Zhang, K., Liu, Z., Traore, D., Yaluk, E., Fu, J. S. and Li, L.: The impact of biogenic emissions on ozone formation in the Yangtze River Delta region based on MEGANv3.1, Air Qual. Atmos. Heal., 14(5), 763–774, doi:10.1007/s11869-021-00977-0, 2021.

Wiedinmyer, C., Akagi, S. K., Yokelson, R. J., Emmons, L. K., Al-Saadi, J. A., Orlando, J. J. and Soja, A. J.: The Fire INventory from NCAR (FINN): A high resolution global model to estimate the emissions from open burning, Geosci. Model Dev., 4(3), 625–641, doi:10.5194/gmd-4-625-2011, 2011.

Yerramilli, A., Challa, V. S., Dodla, V. B. R., Myles, L., Pendergrass, W. R., Vogel, C. A., Tuluri, F., Baham, J. M., Hughes, R., Patrick, C., Young, J. and Swanier, S.: Simulation of surface ozone pollution in the Central Gulf Coast region during summer synoptic condition using WRF/Chem air quality model, Atmos. Pollut. Res., 3(1), 55–71, doi:10.5094/APR.2012.005, 2012.

Zaveri, R. A., Easter, R. C., Fast, J. D. and Peters, L. K.: Model for Simulating Aerosol Interactions and Chemistry (MOSAIC), J. Geophys. Res. Atmos., 113(13), 1–29, doi:10.1029/2007JD008782, 2008.

Zhang, M., Zhao, C., Yang, Y., Du, Q., Shen, Y., Lin, S., Gu, D., Su, W. and Liu, C.: Modeling sensitivities of BVOCs to different versions of MEGAN emission schemes in WRF-Chem (v3.6) and its impacts over eastern China, Geosci. Model Dev., 14(10), 6155–6175, doi:10.5194/gmd-14-6155-2021, 2021.

Zhang, Y., Dubey, M. K., Olsen, S. C., Zheng, J. and Zhang, R.: Atmospheric Chemistry and Physics Comparisons of WRF/Chem simulations in Mexico City with ground-based RAMA measurements during the 2006-MILAGRO. [online] Available from: www.atmos-chem-phys.net/9/3777/2009/ (Accessed 5 May 2022), 2009.

Zhao, C., Huang, M., Fast, J. D., Berg, L. K., Qian, Y., Guenther, A., Gu, D., Shrivastava, M., Liu, Y., Walters, S., Pfister, G., Jin, J., Shilling, J. E. and Warneke, C.: Sensitivity of biogenic volatile organic compounds to land surface parameterizations and vegetation distributions in California, Geosci. Model Dev., 9(5), 1959–1976, doi:10.5194/gmd-9-1959-2016, 2016.

Table 1: The emission activity factors equations referred to MEGAN version 2.04 (M2.04) and the relative updates made for version 2.10 (M2.10)

Emission Activity Factors		M2.04*	M2.10*
Light response		$\gamma_P = 0$ $a < 0 \; a > 180$ $\gamma_P = sin(a)\left[2.46\left(1 + 005 \cdot \left(P_{daily} - 400\right)\right)\varphi \cdot 0.9\,\varphi^2\right]$ $0 < a < 180$	$\gamma_{P,i} = (1 - LDF_i) + LDF_i \cdot \gamma_{P\_LDF}$ $\gamma_{P_{LDF}} = C_P\left[\frac{\alpha \cdot PPFD}{(1 + \alpha^2 \cdot PPFD^2)^{0.5}}\right]$
Temperature response	**Isoprene**	$\gamma_{T,isoprene} = \frac{E_{opt} \cdot CT_2 \cdot exp(CT_1 \cdot x)}{(CT_2 - CT_1 \cdot (1 - exp(CT_2 \cdot x)))}$ Note, CT are fixed values	$\gamma_{T,i} = (1 - LDF_i) \cdot \gamma_{T\_LIF,i} + LDF_i \cdot \gamma_{T\_LDF,i}$ $\gamma_{T_{LDF},i} = E_{opt} \cdot \left[CT_2 \cdot \frac{e^{(CT_{1,i} \cdot x)}}{CT_2 - CT_{1,i} \cdot (1 - e^{(CT_2 \cdot x)})}\right]$ $\gamma_{T_{LIF,i}} = e^{(\beta_i (T - T_S))}$
	Non isoprene compounds	$\gamma_T = e^{(\beta_i (T - T_S))}$	Note, CT values have been updated
Leaf age response		$\gamma_{age} = F_{new}A_{new} + F_{gro}A_{gro} + F_{mat}A_{mat} + F_{old}A_{old}$	
		Anew, Agro, Amat, and Aold are fixed values	Anew, Agro, Amat, and Aold updated using Table 4 of G12
Soil moisture response	**Isoprene**	$\gamma_{SM} = 1$	$\gamma_{SM,isoprene} = 1 \quad (\theta > \theta_1)$ $\gamma_{SM,isoprene} = \frac{\theta - \theta_W}{\Delta\theta_1} \quad (\theta_W < \theta < \theta_1)$ $\gamma_{SM,isoprene} = 0 \quad (\theta < \theta_W)$
	Non isoprene compounds		$\gamma_{SM} = 1$
Canopy environment response		$\gamma_{LAI} = \frac{0.49 LAI_C}{[(1 + 0.2 LAI_C^2)^{0.5}]}$	$\gamma_{LAI} = LAI \cdot C_{CE}$

*See text for definitions of variables.

Table 2: Biogenic emission classes and emission factors (new and old) (μg m^{-2} hr^{-1}) for each plant functional types updated to MEGAN v2.10 applied to WRF-Chem (G12).

	BT_2.04	BT_2.10	NT_2.04	NT_2.10	SB_2.04	SB_2.10	HB_2.04	HB_2.10
Isoprene	13000	9000	2000	1800	11000	3333	400	866
Myrcene	20	50	75	70	22	36	0.3	0.3
Sabinene	45	62	70	70	50	56	0.7	0.7
Limonene	45	80	100	100	52	73	0.7	0.7
3-Carene	18	34	160	160	25	53	0.3	0.3
t-β-Ocimene	90	132	60	70	85	110	1	2
β-Pinene	90	126	300	300	100	116	1.5	1.5
α-Pinene	180	480	450	500	200	233	2	2
Other Monoterpenes	90	150	180	180	110	140	4.8	5
α-Farnesene	35	48	30	40	30	40	0.50	3
β-Caryophyllene	30	48	60	80	45	50	0.90	1
Other Sesquiterpenes	75	108	110	120	85	100	1.40	2
232-MBO	0.1	0.41	100	380	1	0.01	0.01	0.01
Methanol	800	740	800	900	800	900	800	500
Acetone	240	240	240	240	240	240	80	80
CO	1000	600	1000	600	1000	600	1000	600
Bidirectional VOC	1000	500	1000	500	1000	500	1000	80
Stress VOC	1000	280	1000	300	1000	300	1000	300
Other VOC	1000	140	1000	140	1000	140	1000	140

Table 3: Namelist settings of the physical parameterizations used in the WRF-Chem setup simulations.

Model scheme		Reference
Microphysics	Morrison two moment	(Morrison et al., 2009)
Longwave radiation	RRTMG	(Iacono et al., 2008)
Shortwave radiation	RRTMG	(Iacono et al., 2008)
PBL model	MYJ	(Janjić, 1994)
Land surface	Unified Noah land-surface	(Chen et al., 1996)
Cumulus parameterization	Grell-Freitas	(Grell and Freitas, 2014)
Gas phase chemical mechanism	MOZART version 4.0	(Emmons et al., 2010)
Aerosols representation	4-bin MOSAIC	(Zaveri et al., 2008)

845

Table 4: Simulations performed in this study.

Model run*	Emission activity factors (γ_i) modified	PFTs emission factors updated	Isoprene emission factor calculated by the MEGAN algorithm
M2.04	No	No	No
MG	Yes	No	No
MGPFT	Yes	Yes	No
M2.10	Yes	Yes	Yes

*M2.04 = MEGAN v2.04, MG = only activity factors updated, MGPFT = activity factors and PFT emission factors updated, M2.10 = MGPFT plus including the update to the isoprene emission factor.

850

855

Table 5: Summary of the statistics between predicted and measured O_3, NO_2 and CO concentrations from the Airbase dataset (intended as daytime hours weekly mean from August 10th, 2015 at 0000 UTC to August 16th, 2015 at 0000 UTC), namely the (a) normalized mean bias (bias - %), (b) normalized root mean square errors (nrmse – dimensionless), (c) the correlation coefficient (r - dimensionless), and the relative number of points analysed (n_{XY}). Values are shown according to the different station areas: suburban (SUB), urban (URB) and rural (RUR), and the different WRF-Chem model runs (control simulation - M2.04, activity factors updated - MG, PFTs emission factors updated - MGPFT, and the isoprene emission factor updated - M2.10).

	O_3			NO_2			CO		
	SUB	**URB**	**RUR**	**SUB**	**URB**	**RUR**	**SUB**	**URB**	**RUR**
n_{XY}	515	891	576	592	1602	487	151	637	73
bias_M2.04	26	31	15	-39	-63	-3	-27	-35	-29
bias_MG	37	41	24	-39	-63	-2	-23	-31	-26
bias_MGPFT	37	41	24	-39	-63	-3	-23	-31	-26
bias_M2.10	36	41	23	-39	-63	-2	-23	-32	-26
nrmse_ M2.04	0.34	0.39	0.23	0.82	0.96	0.89	0.71	0.80	0.71
nrmse_MG	0.43	0.49	0.30	0.82	0.96	0.90	0.70	0.78	0.70
nrmse_ MGPFT	0.43	0.49	0.30	0.82	0.96	0.90	0.70	0.78	0.70
nrmse_ M2.10	0.42	0.48	0.29	0.81	0.96	0.90	0.70	0.78	0.70
r_ M2.04	0.75	0.75	0.84	0.24	0.22	0.43	0.11	0.20	-0.02
r_MG	0.77	0.76	0.85	0.24	0.22	0.43	0.12	0.22	0.00
r_ MGPFT	0.77	0.76	0.85	0.24	0.22	0.43	0.12	0.22	0.00
r_ M2.10	0.78	0.76	0.86	0.24	0.22	0.43	0.12	0.21	0.00

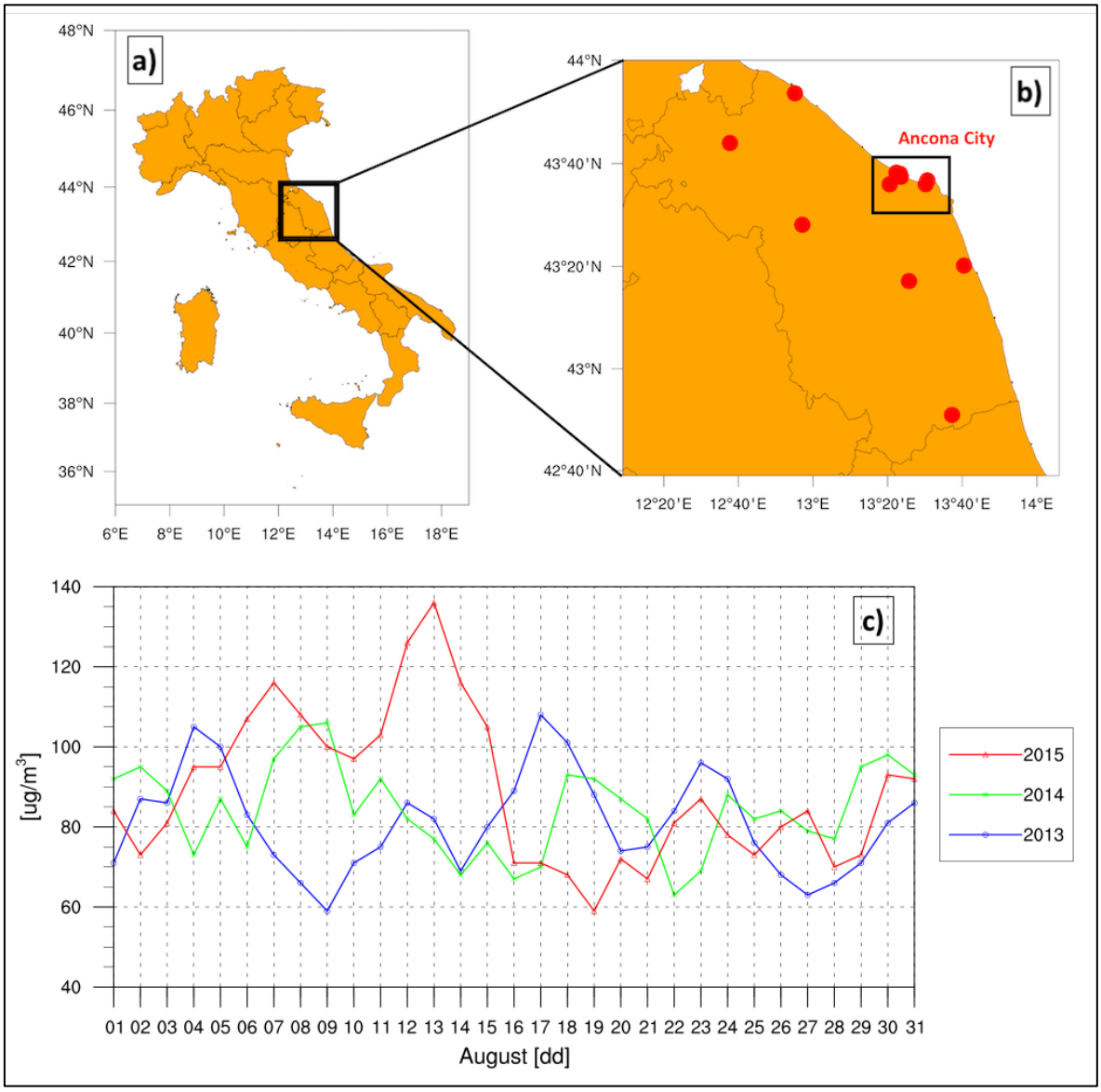

Figure 1: (a-b) Marche region (Italy) air quality monitoring stations analysed in the 3 years study. (c) The ozone maximum daily eight-hour mean (ug m^{-3}), averaged over all stations (b), in the month of August 2013, 2014 and 2015 (http://94.88.42.232:16382 - ARPAM).

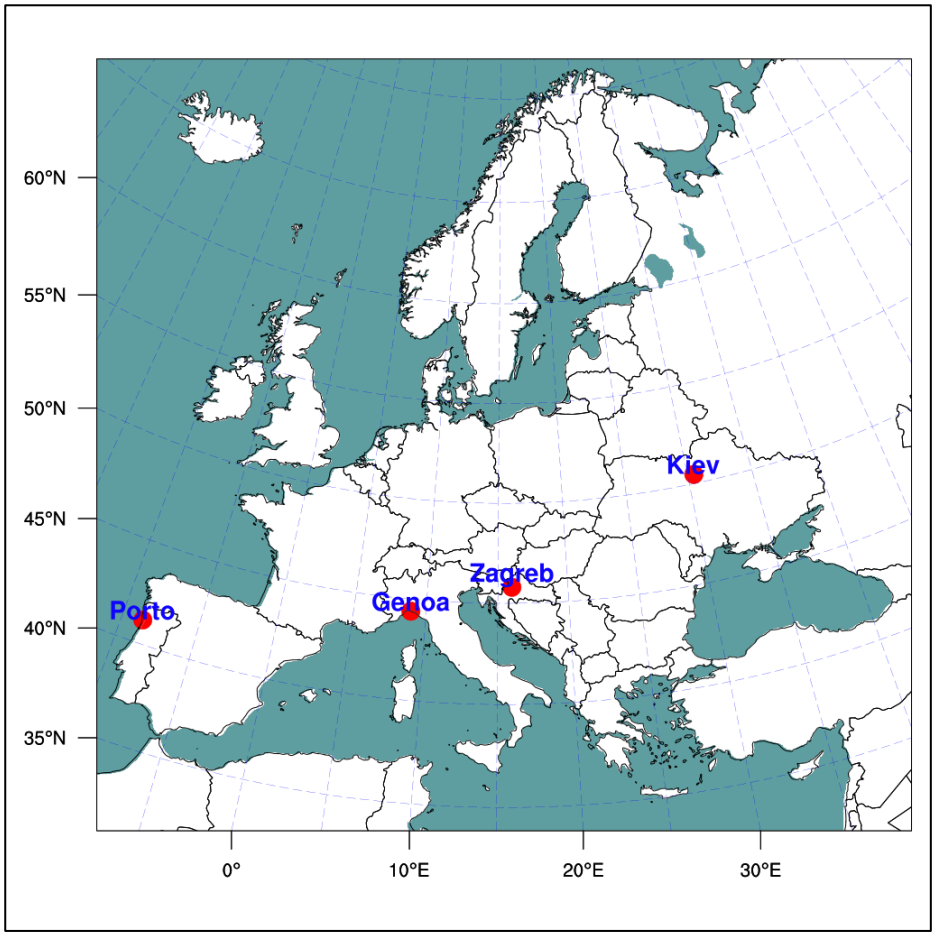

Figure 2: The numerical domain of the WRF-Chem simulations with 380×360 grid points and 12 km grid cells and the location of the four cities in Europe selected for analyzing the simulated isoprene and α-pinene emissions, namely Porto (Portugal), Genoa, (Italy), Zagreb, (Croatia), and Kiev, (Ukraine) spanning in the range 41.15-51.45 °N and 8.63° W-30.50° E.

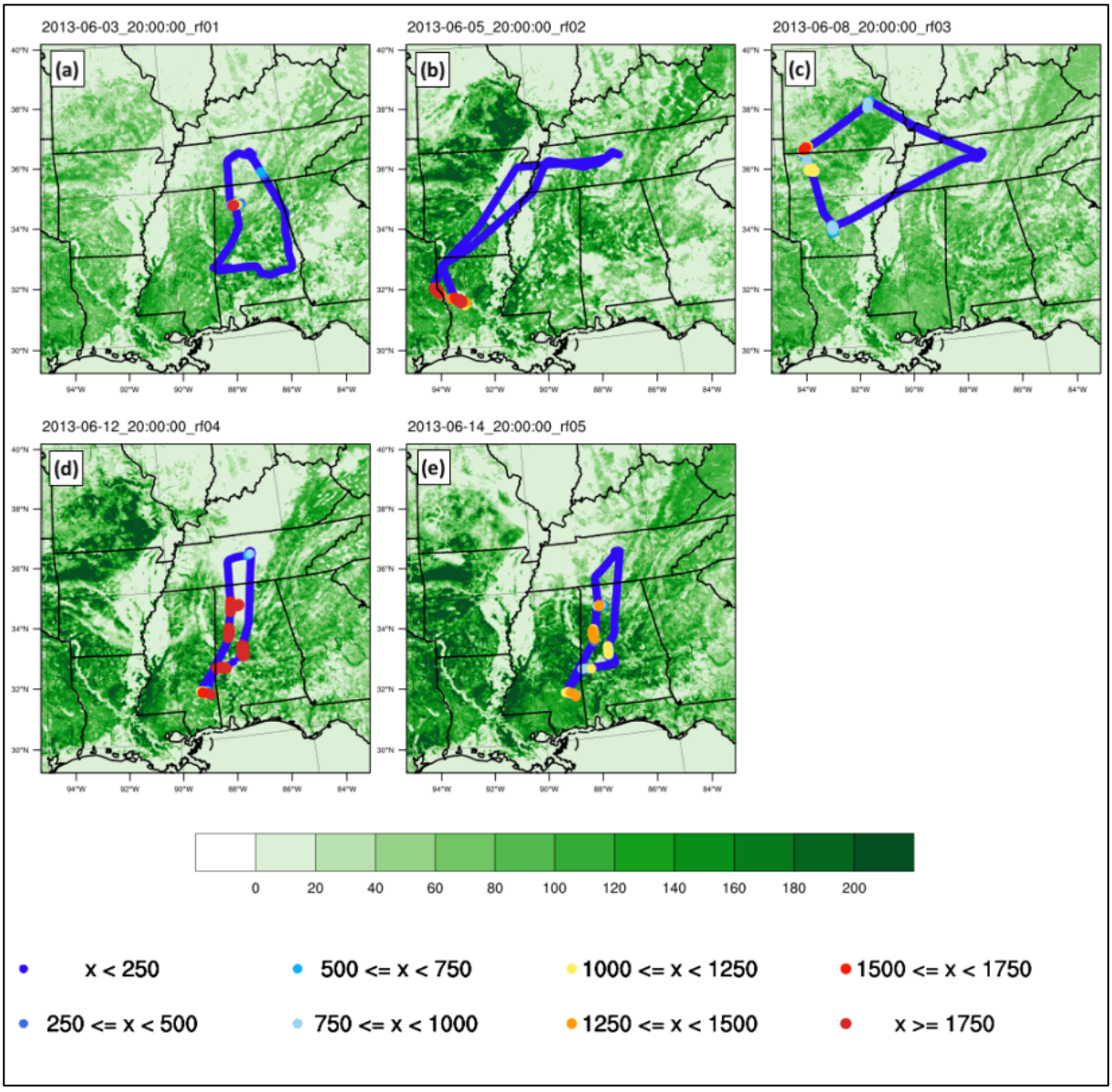

Figure 3: The x values (i.e., colored dots) denote the isoprene mixing ratios (pptv) along the aircraft flight tracks plotted over the different maps of isoprene emission factors (mol km-2 h-1) from M2.04 simulation. Results are for each research flight day at 3:00 pm local time (20:00 UTC), namely (a) rf01: 03/6/13; (b) rf02: 05/6/13; (c) rf03: 08/6/13; (d) rf04: 12/6/13; (e) rf05: 14/6/13.

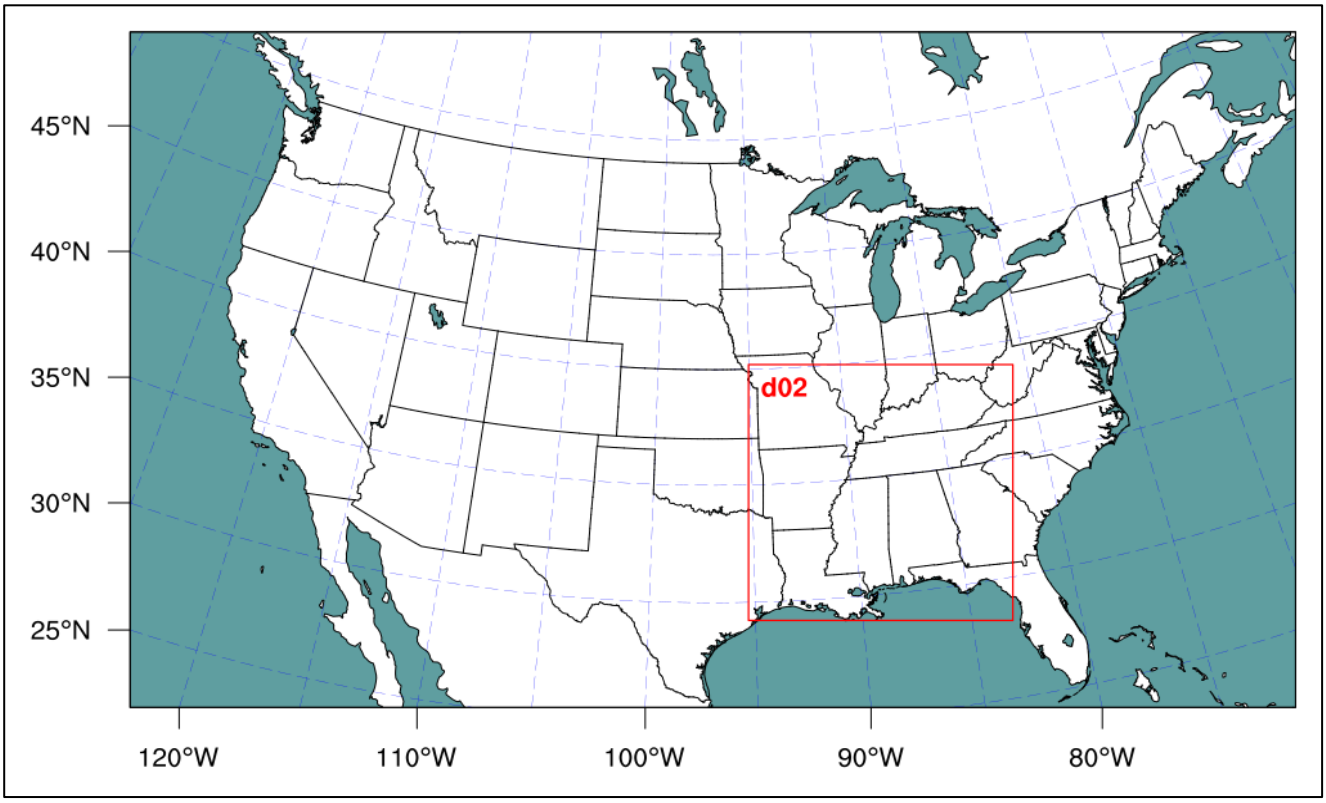

Figure 4: The numerical domains of the NOMADSS simulations: the coarse domain has 442×265 grid points with 12 km grid cells, the nested domain, with 4 km grid cells, has 301×301 grid points.

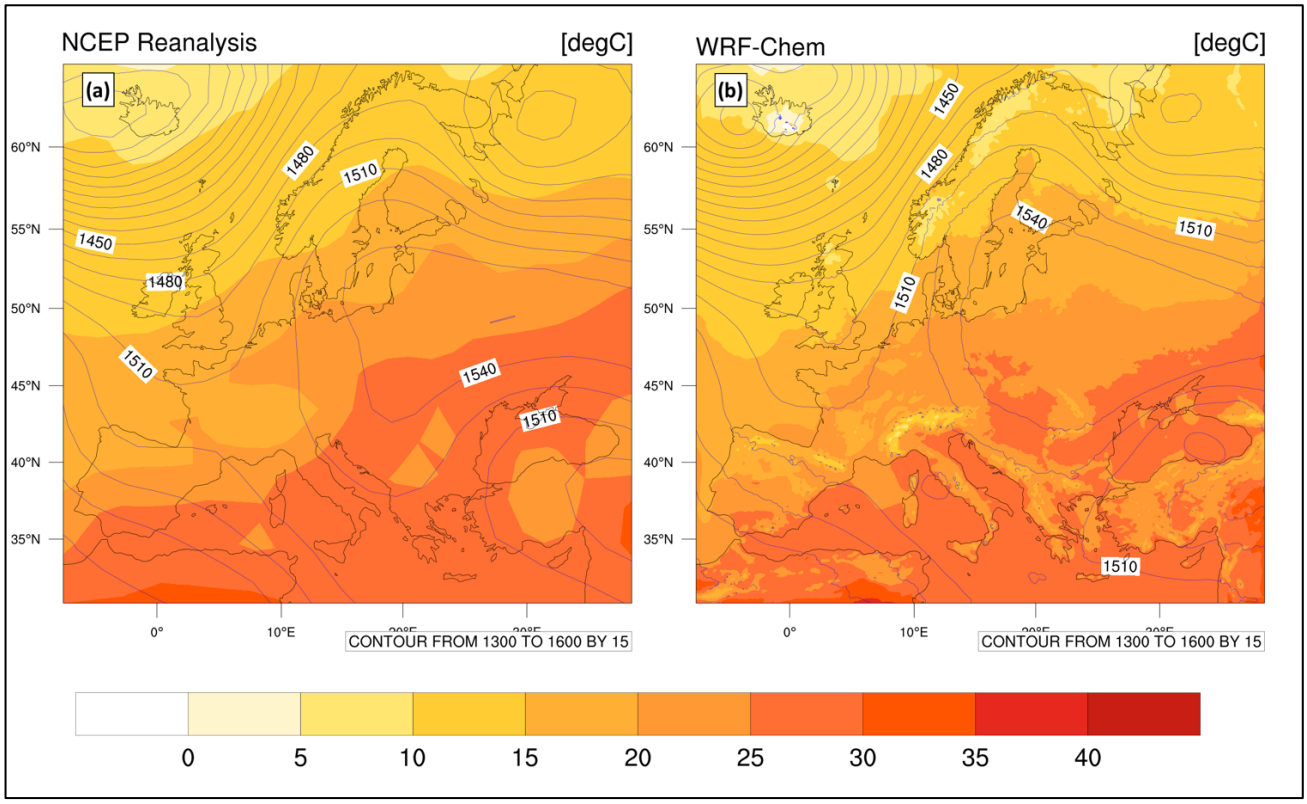

Figure 5: Comparison between the 6-day (August 10th – 15th, 2015) average geopotential height (m) at 850 hPa and mean temperature at 995 hPa, obtained with (a) NCAR/NCEP reanalysis and (b) the WRF-Chem model.

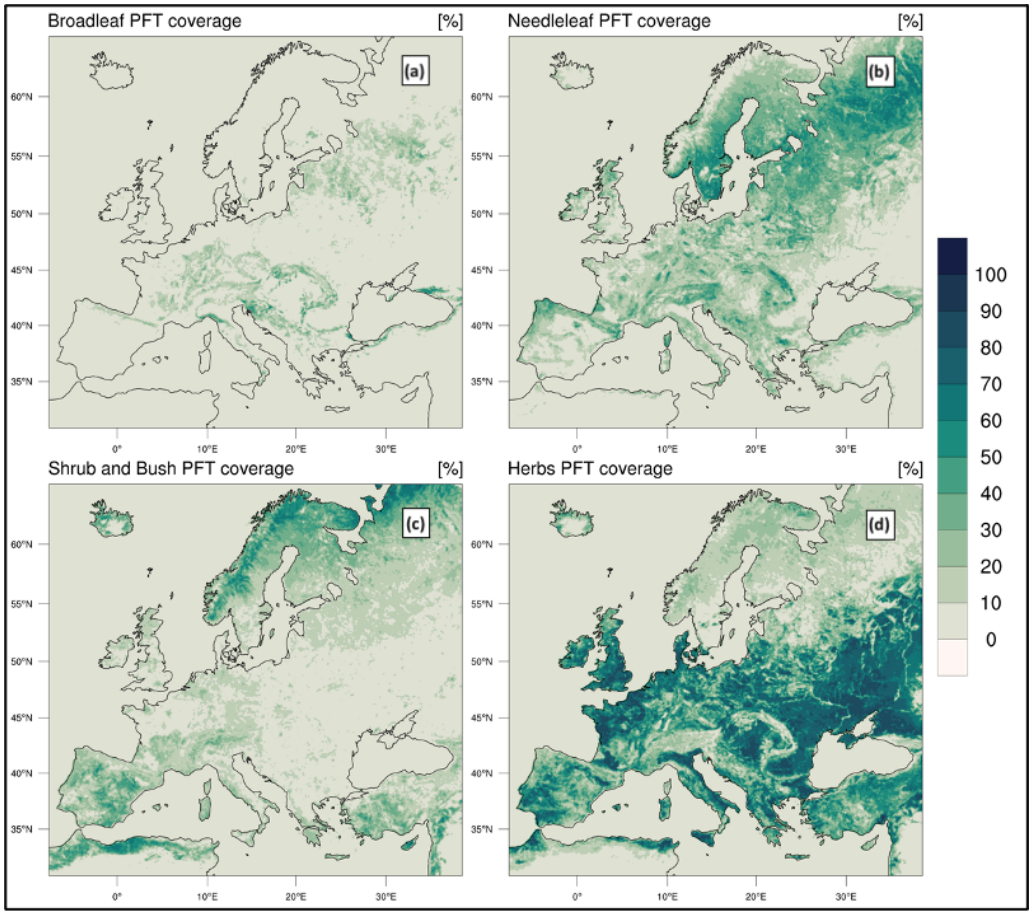

Figure 6: Percentage coverage (%) of plant functional types (PFTs) classification included into MEGAN database, computed in August 2015. From the upper left map: (a) coverage of broadleaf trees (PFTP_HB), (b) needleleaf trees (PFTP_NB), broadleaf shrubs (PFTP_SB), and (d) grass and other (PFTP_HB).

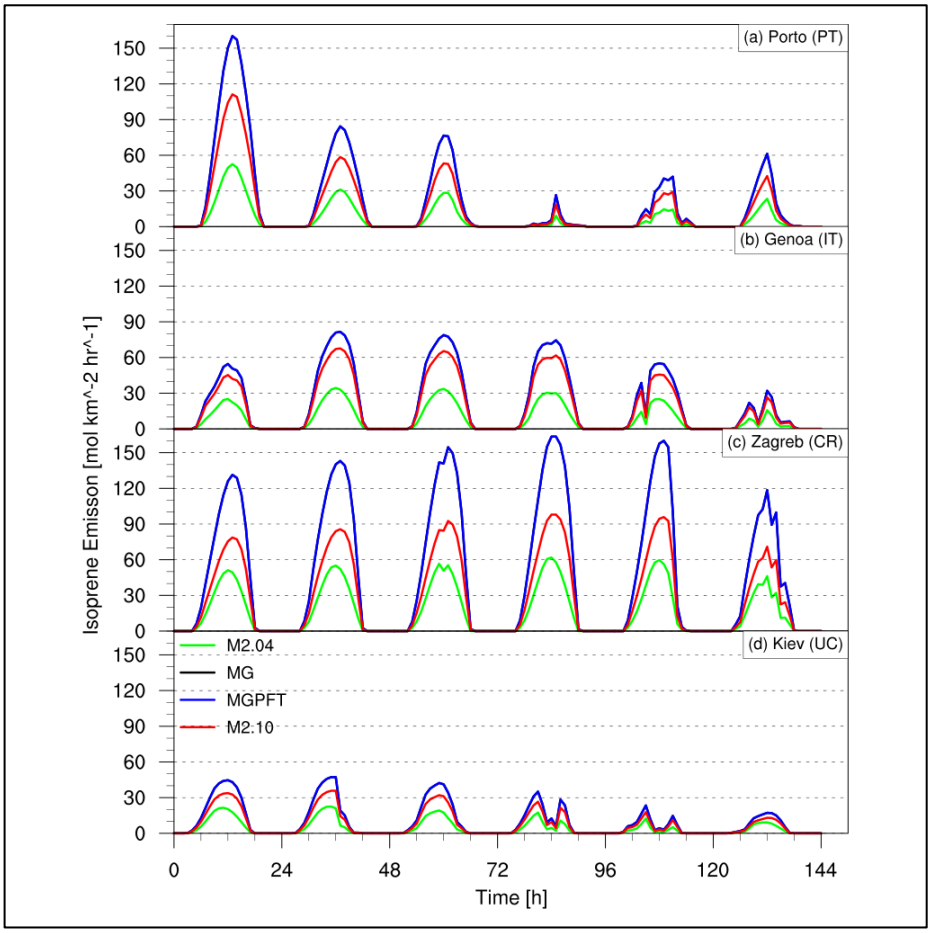

Figure 7: Time series of isoprene emissions (mol km^{-2} hr^{-1}) for different MEGAN algorithm configurations evaluated in 4 cities in Europe, namely (a) Porto, Portugal; (b) Genoa, Italy; (c) Zagreb, Croatia; (d) Kiev, Ukraine. The time period considered is from August 10th, 2015 at 0000 UTC to August 16th, 2015 at 0000 UTC. The green lines represent the control simulation (M2.04), the black lines indicate the activity factors (γ) updates (MG), the blue lines are representative of the PFTs emission factors updates (MGPFT), and the red lines show the isoprene emission factor as the emission factor of all the other compound classes (M2.10).

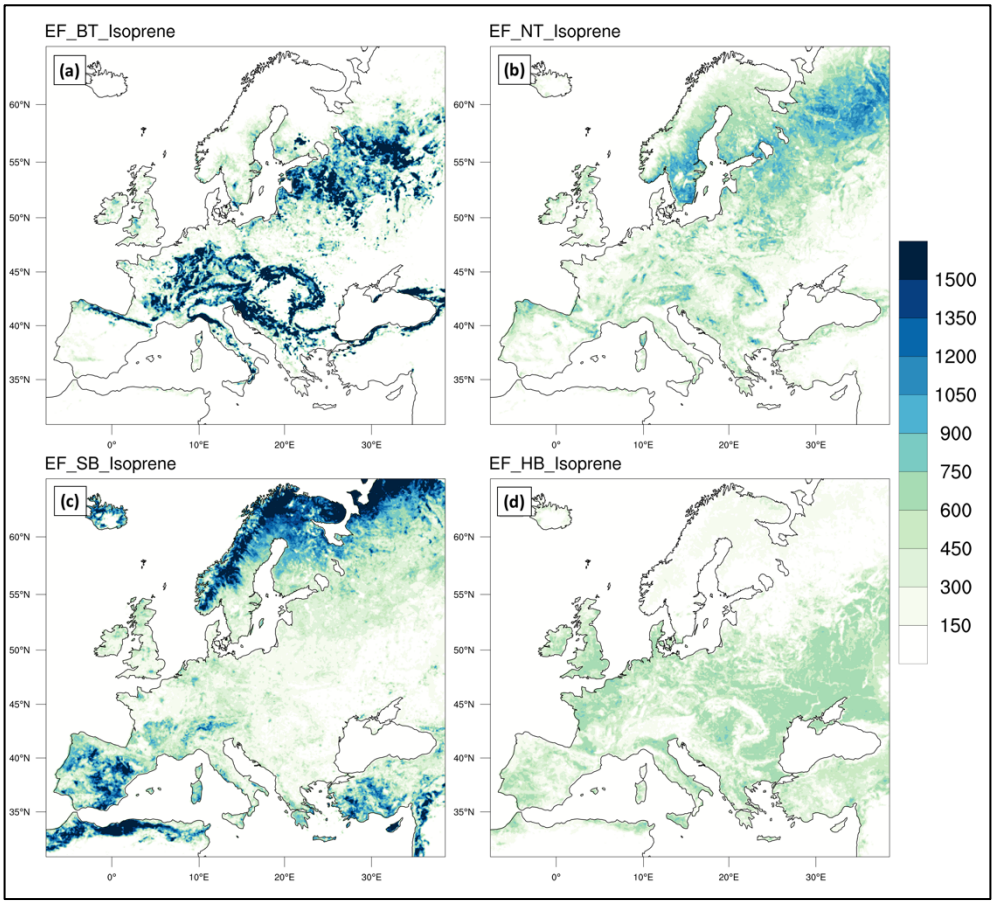

Figure 8: Plant functional type (PFT) weighted emission factor (PFT emission factor and PFT percentage) (ug km^{-2} hr^{-1}) of isoprene, computed for the month of August 2015 in Europe. The emission factor values used are from Table 2 (2.10 column). From the upper left map: (a) PFT weighted emission factor of broadleaf trees (PFTP_BT), (b) needleleaf trees (PFTP_NB), broadleaf shrubs (PFTP_SB), and (d) grass and other (PFTP_HB).

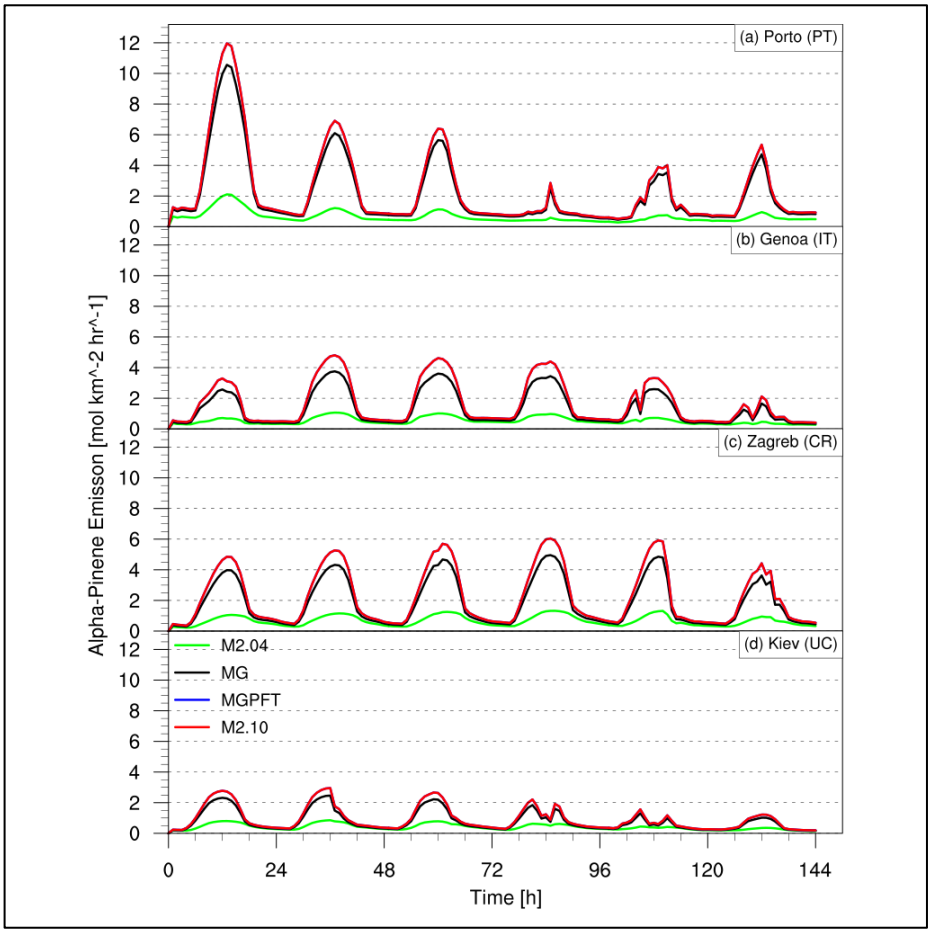

Figure 9: Time series of α-pinene emissions (mol km^{-2} hr^{-1}) for different MEGAN algorithm configurations evaluated in 4 cities in Europe, namely (a) Porto, Portugal; (b) Genoa, Italy; (c) Zagreb, Croatia; (d) Kiev, Ukraine. The time period considered is from August 10th, 2015 at 0000 UTC to August 16th, 2015 at 0000 UTC. The green lines represent the control simulation (M2.04), the black lines indicate the activity factors (γ_i) updates (MG), the blue lines are representative of the PFTs emission factors updates (MGPFT), and the red lines show the isoprene emission factor as the emission factor of all the other compound classes (M2.10).

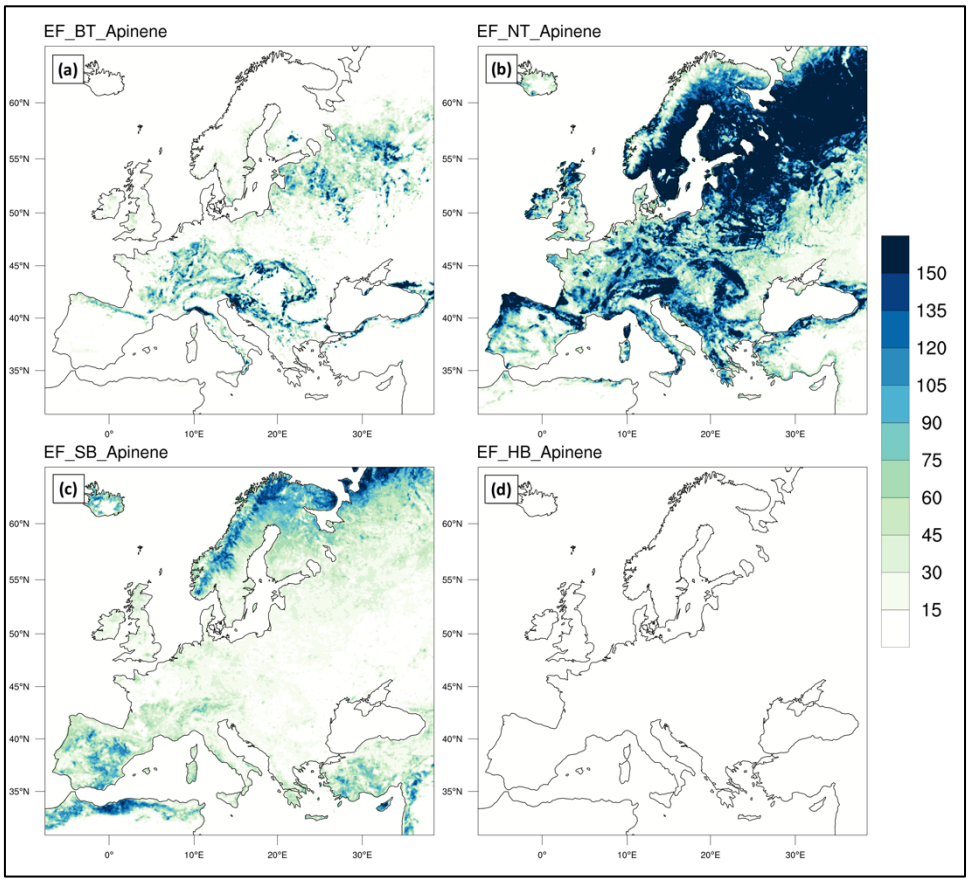

Figure 10: Plant functional type (PFT) weighted emission factor (PFT emission factor and PFT percentage) (ug km^{-2} hr^{-1}) of α-pinene, computed for the month of August 2015 in Europe. The emission factor values used are from Table 2 (2.10 column). From the upper left map: (a) PFT weighted emission factor of broadleaf trees (PFTP_BT), (b) needleleaf trees (PFTP_NB), broadleaf shrubs (PFTP_SB), and (d) grass and other (PFTP_HB).

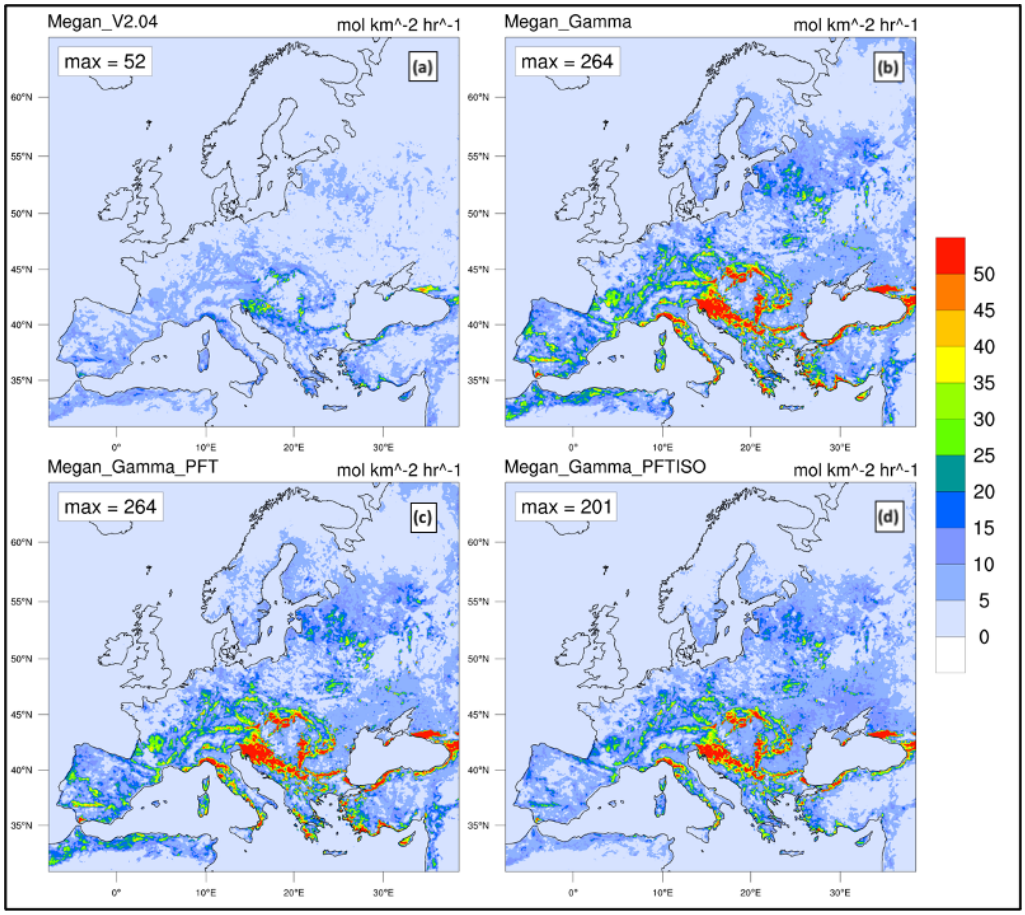

940 **Figure 11: The spatial distribution of isoprene emission (mol km^{-2} hr^{-1}) calculated as average in the time period from August 10, 2015 at 0000 UTC to August 16, 2015 at 0000 UTC for the different MEGAN configurations, namely (a) control simulation (M2.04), (b) activity factors (γ_i) updated (MG), (c) PFTs emission factors updated (MGPFT), and (d) the isoprene emission factor updated (M2.10).**

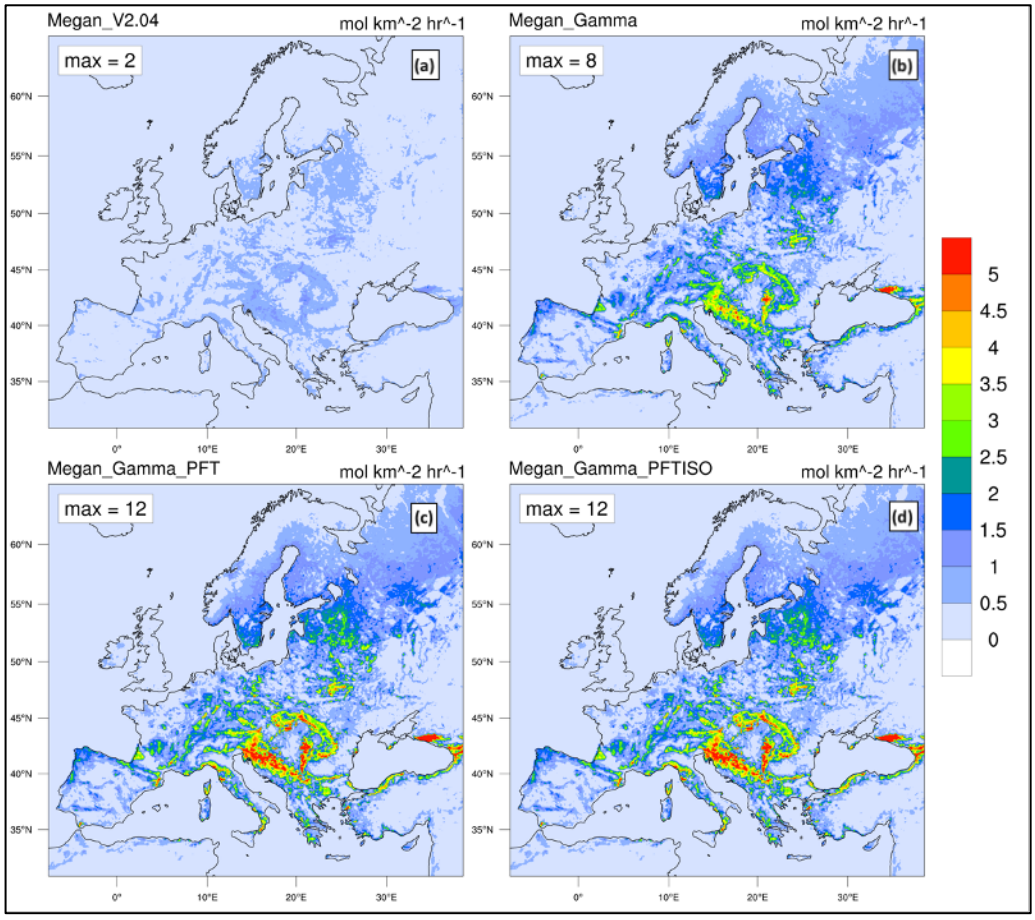

945 **Figure 12: The spatial distribution of α-pinene emission (mol km^{-2} hr^{-1}) calculated as weekly average (from August 10, 2015 at 0000 UTC to August 16, 2015 at 0000 UTC) for the different MEGAN configurations, namely (a) control simulation (M2.04), (b) activity factors (γ_i) updated (MG), (c) PFTs emission factors updated (MGPFT), and (d) the isoprene emission factor updated (M2.10).**

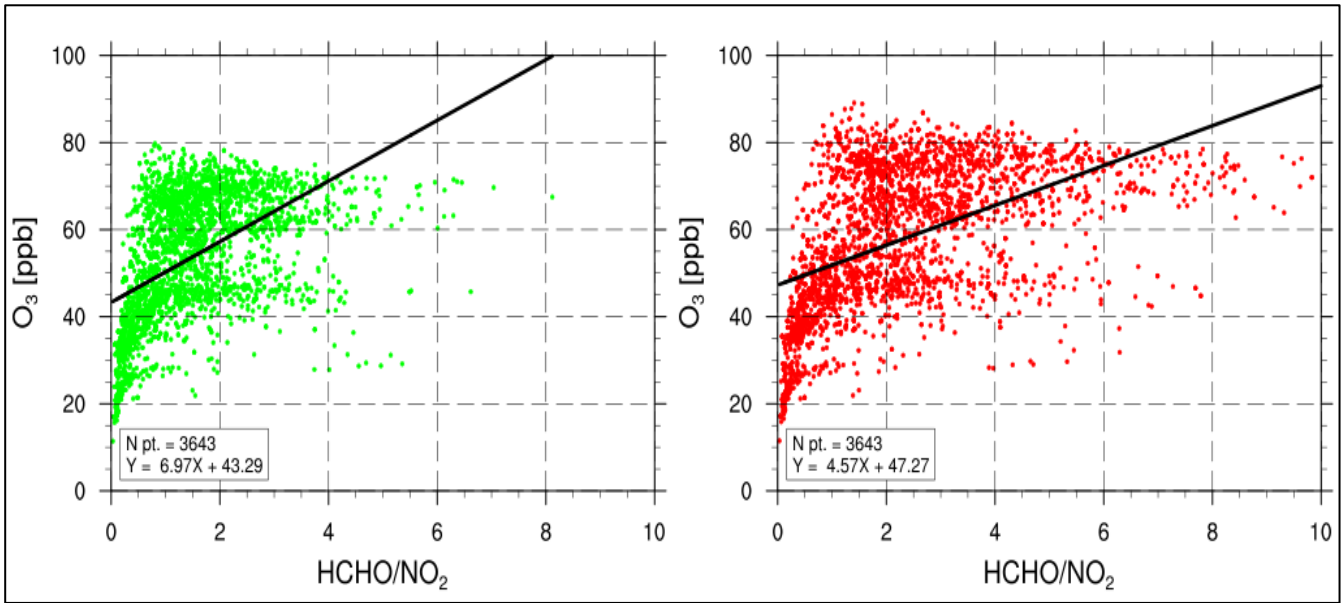

Figure 13: Scatter plot and linear regression of O_3 bias versus the ratio of $HCHO/NO_2$ for the simulations M2.04 (green dots) and M2.10 (red dots). Each plot shows the number of ground-based monitoring observations (N pt.) from the Airbase database and equation for the line of best fit (Y).

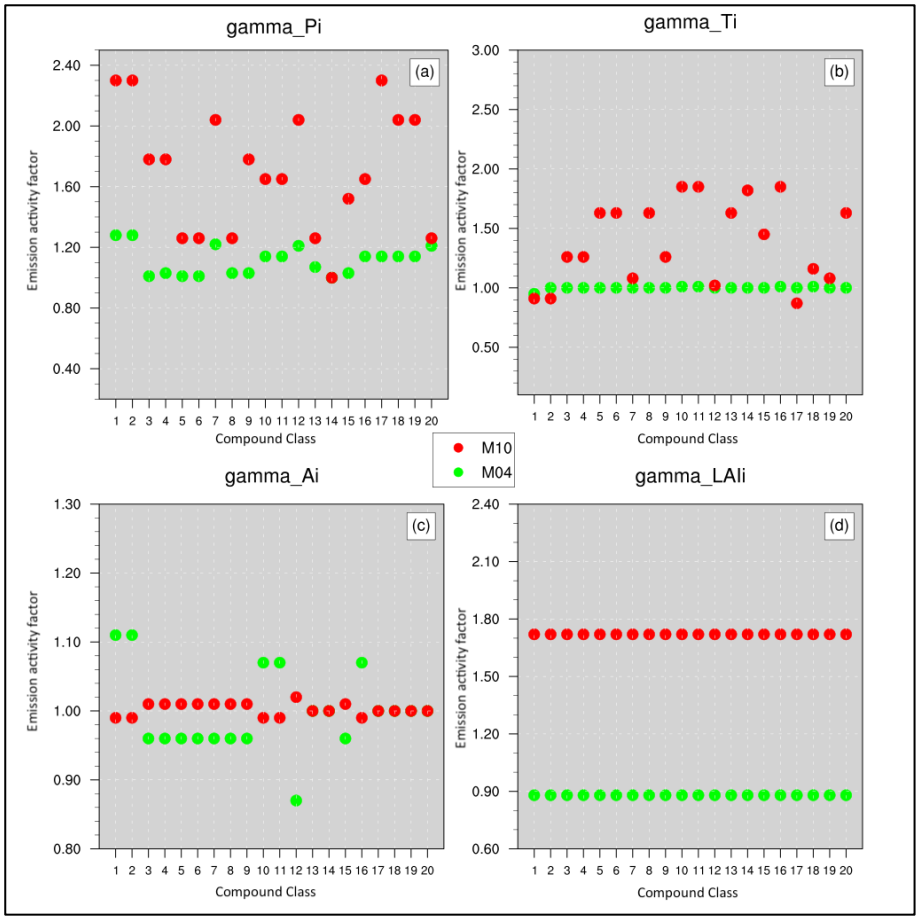

Figure 14: Emission activity factors (y-axis, dimensionless) from M2.04 (M04) and M2.10 (M10) for different compound classes (1. Isoprene, 2. Myrcene, 3. Sabinene, 4. Limonene, 5. 3-Carene, 6. t-β-Ocimene, 7. β-Pinene, 8. α-Pinene, 9. Other Monoterpenes, 10. α-Farnesene, 11. β-Caryophyllene, 12. Other Sesquiterpenes, 13. 232-MBO, 14. Methanol, 15. Acetone, 16. Carbon monoxide, 17. Nitric oxide, 18. Bidirectional VOC, 19. Stress VOC and 20. other VOC). Each panel is for a different meteorological factor: (a) photosynthetic photon flux density (γ_P, GAMMA_P), (b) temperature (γ_T, GAMMA_T), (c) leaf age (γ_{age}, GAMMA_A), and (d) leaf area index (γ_{LAI}, GAMMA_LAI). The factors refer to the city of Genoa (Italy) on August 13th (12:00 UTC), 2015.

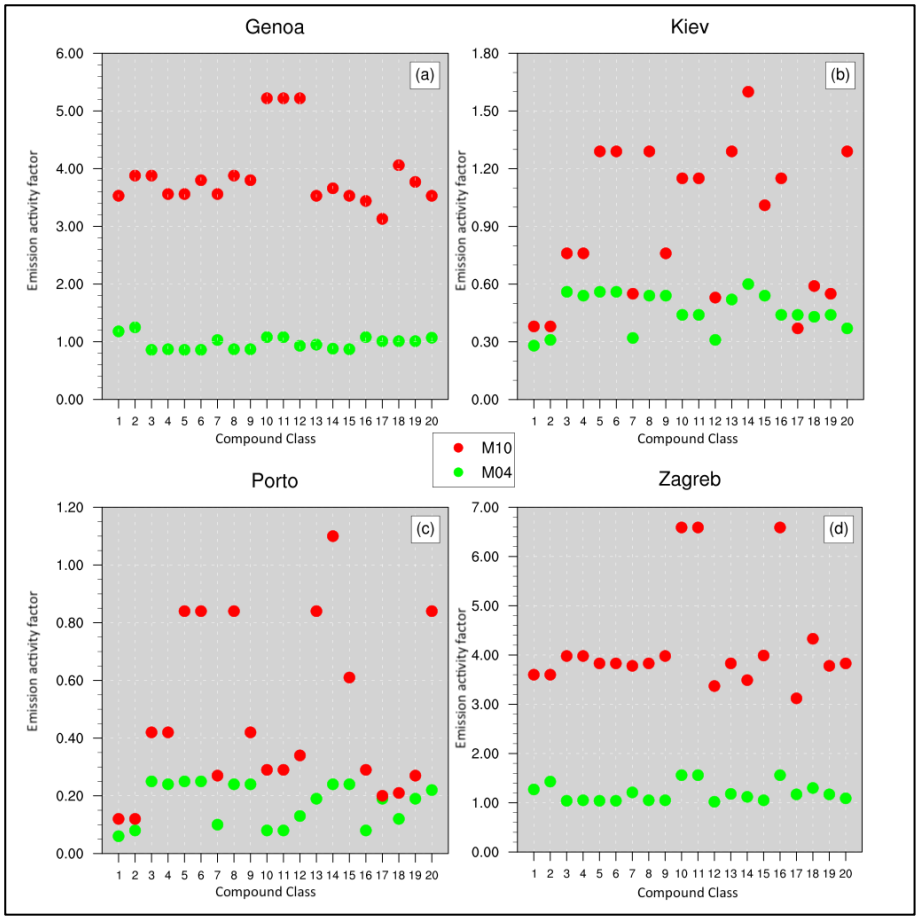

Figure 15: Total emission activity factors (y-axis, dimensionless) from M2.04 (M04) and M2.10 (M10) runs for different compound classes (i.e. 1. Isoprene, 2. Myrcene, 3. Sabinene, 4. Limonene, 5. 3-Carene, 6. t-β-Ocimene, 7. β-Pinene, 8. α-Pinene, 9. Other Monoterpenes, 10. α-Farnesene, 11. β-Caryophyllene, 12. Other Sesquiterpenes, 13. 232-MBO, 14. Methanol, 15. Acetone, 16. Carbon monoxide, 17. Nitric oxide, 18. Bidirectional VOC, 19. Stress VOC and 20. other VOC). Each panel is for different city: (a) Genoa (Italy), (b) Kiev (Ukraine), (c) Porto (Portugal), and (d) Zagreb (Croatia), on August 13th (12:00 UTC), 2015.

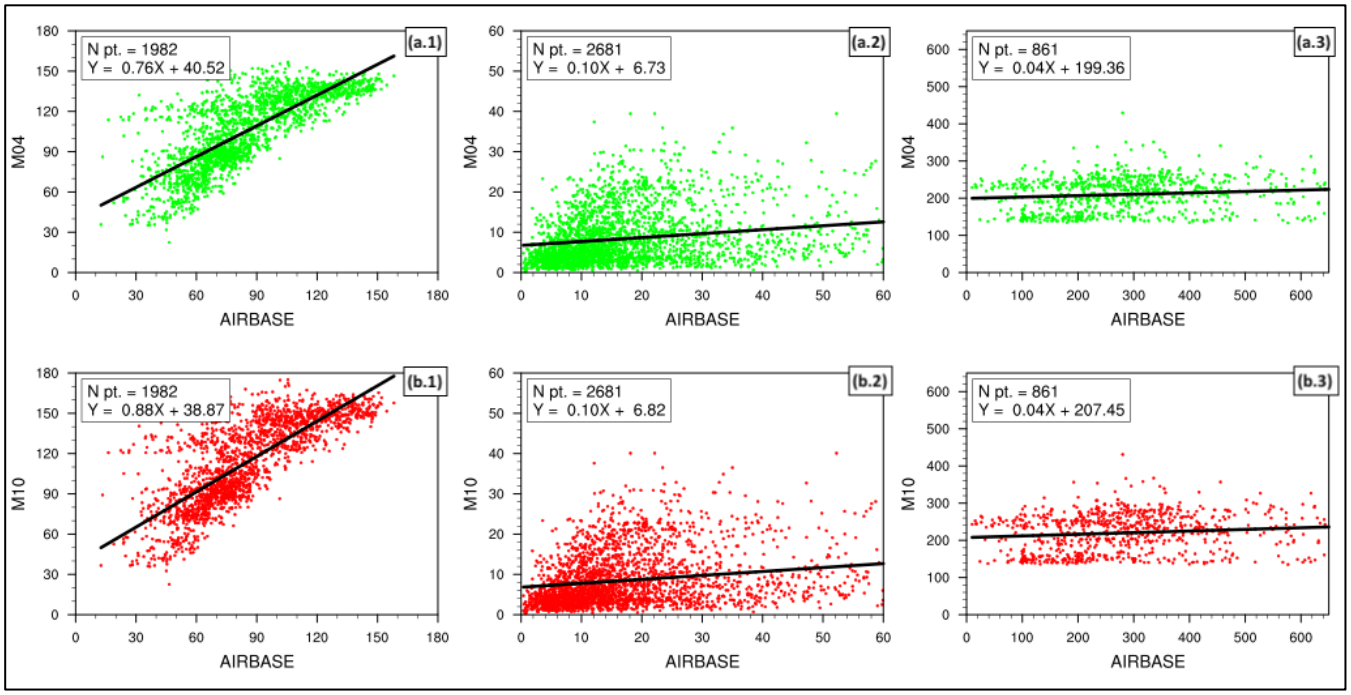

980

Figure 16: Scatter plot and linear regression for the simulations M2.04 (M04 - a-green dots) and M2.10 (M10 - b-red dots) against the observed (AirBase dataset) concentrations (μg m^{-3}) of (1) ozone, (2) nitrogen dioxide and (3) carbon monoxide. Each plot shows the number of points recorded (N pt.), and equation for the line of best fit (Y). The values shown are the 8-hour daytime average, weekly mean from August 10th, 2015 at 0000 UTC to August 16th, 2015 at 0000 UTC.

985

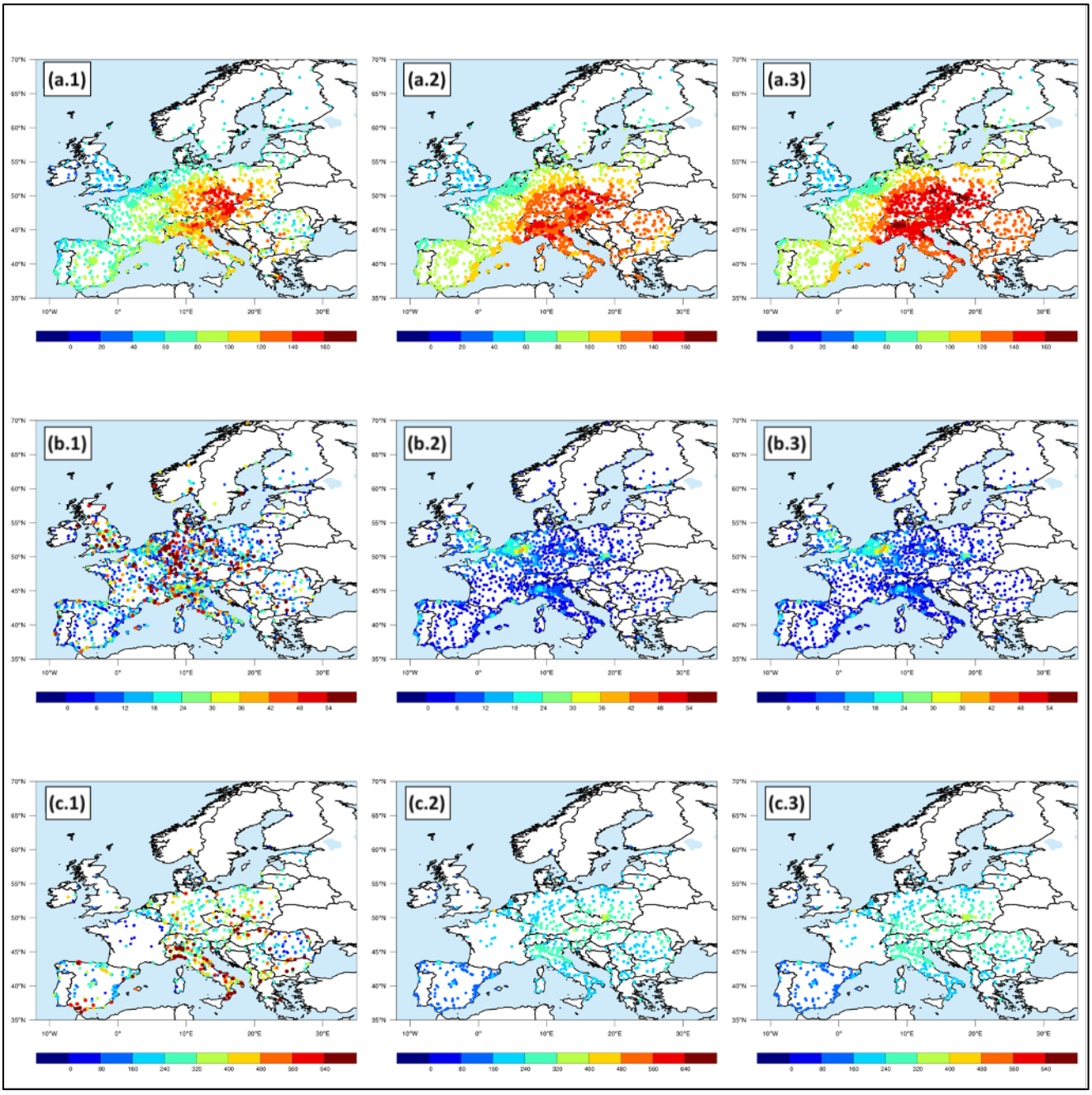

Figure 17: Comparison between the (1) AIRBASE dataset of the mean day time (7 am – 6 pm UTC), (2) control simulation (M2.04 run) and (3) M2.10 run with all the MEGAN code updates concentrations of (A) O_3, (B) CO, and (C) NO_2 over the period from August 10th 00:00 UTC to 16th 00:00 UTC, 2015.

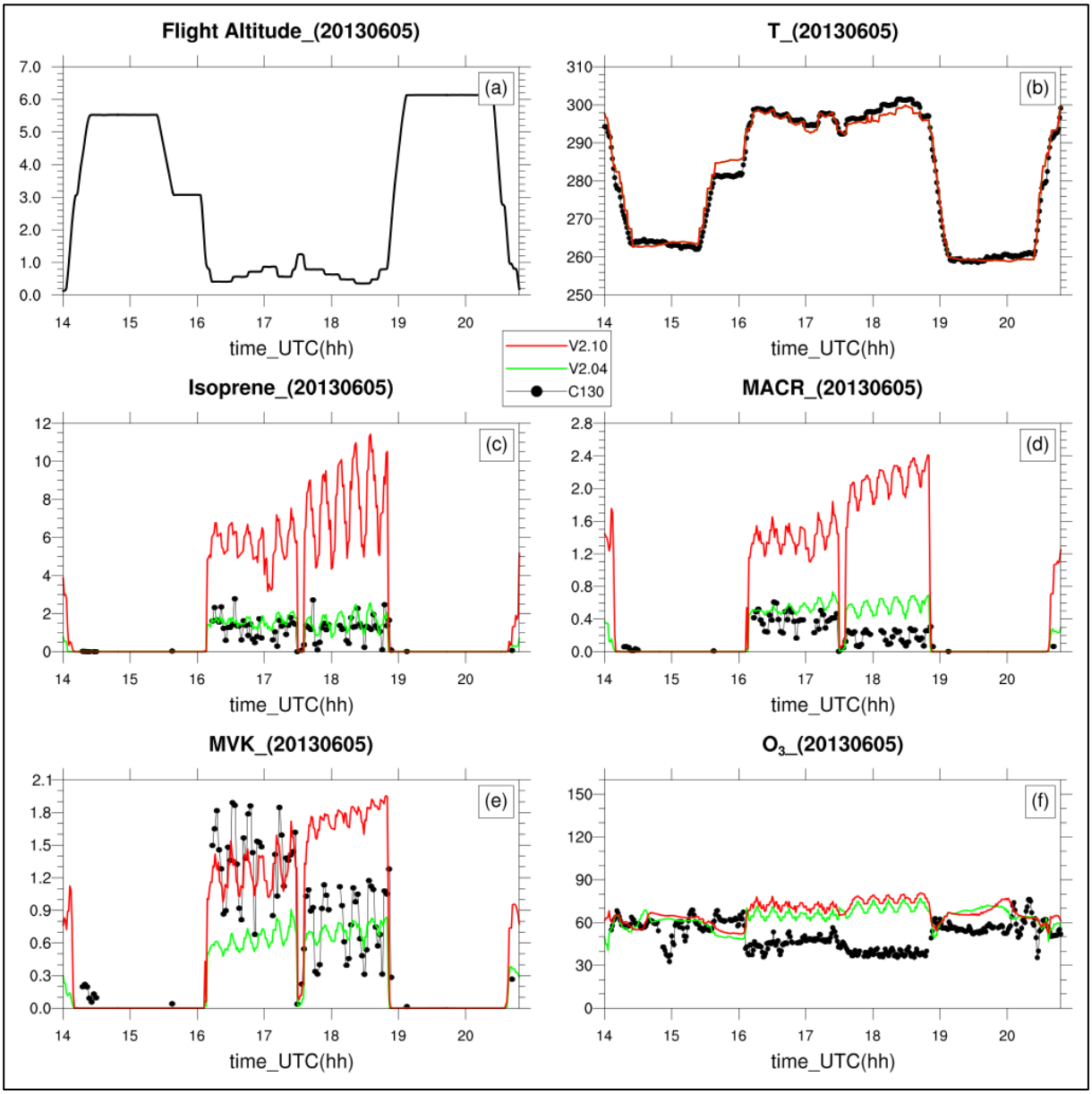

Figure 18: The flight altitude (a - km), the temperature (b - K), the concentration of isoprene (c - ppb), methacrolein (MACR) (d - ppb), methyl vinyl ketone (MVK) (e – ppb), and ozone (f - ppb), for the second NOMADSS flight (rf02). The black line shows the C-130 aircraft measurements, the green and red lines indicate the WRF-Chem model results using MEGAN version 2.04 (M2.04 run) and MEGAN updated to the version 2.10 (M2.10 run), respectively. In panel b) the green line is not showed since it is overlapped by the red line, they have identical values.

Supplemental materials for "Comparison and evaluation of updates to WRF-Chem (v3.9) biogenic emissions using MEGAN"

Table S1: Soil-related wilting point (θ_w) (m^3 m^{-3}) used by MEGAN soil moisture emission activity factor. Adapted from Chen and Dudhia, 2001.

Soil type	Wilting point
Sand	0.01
Loamy sand	0.028
Sandy loam	0.047
Silt loam	0.084
Silt	0.084
Loam	0.066
Sandy clay loam	0.067
Silty clay loam	0.12
Clay loam	0.103
Sandy clay	0.1
Silty clay	0.126
Clay	0.138
Organic material	0.06
Water	n.a.
Bedrock	0.094
Other (land–ice)	0.028

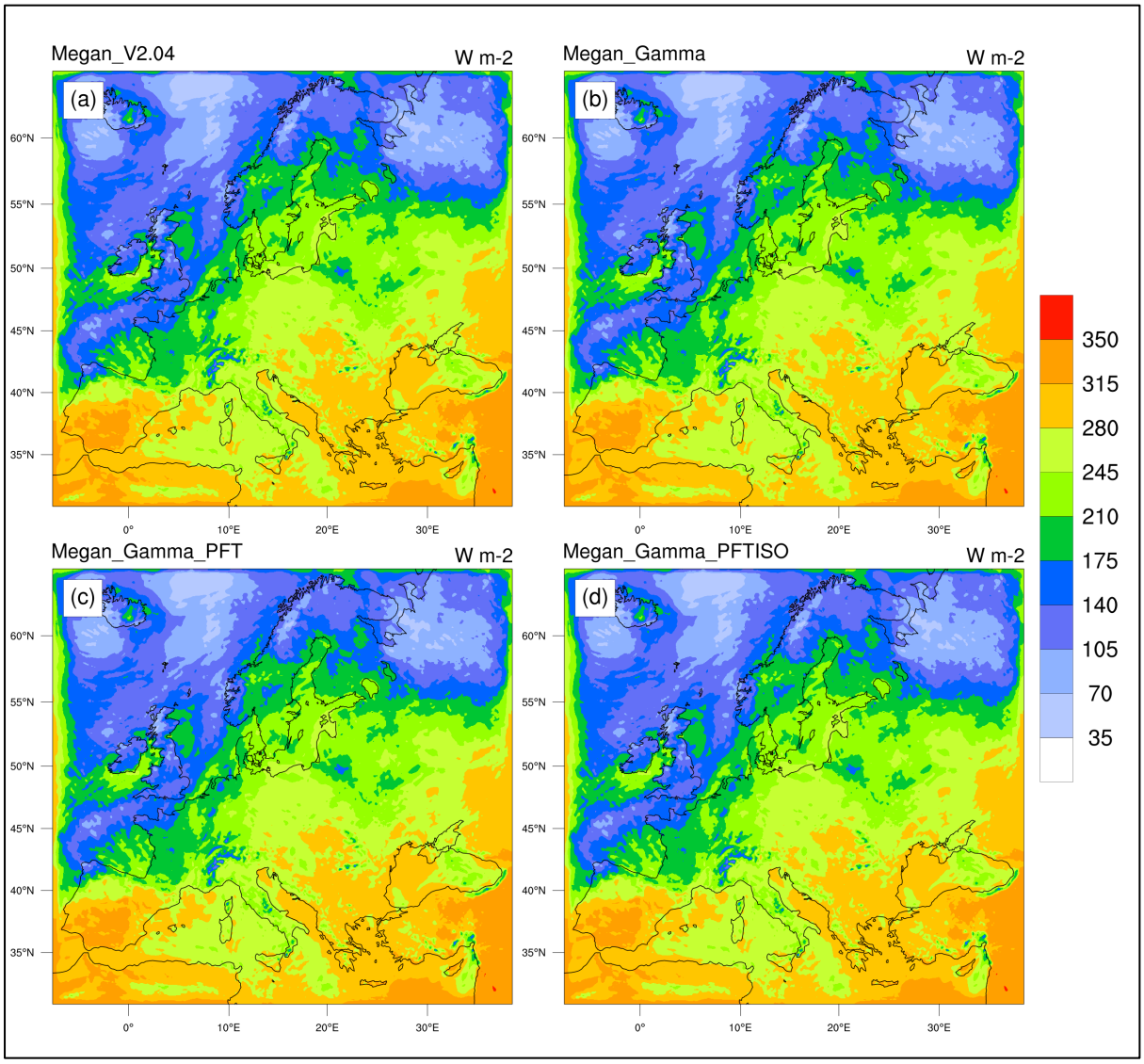

Figure S1: Downward shortwave radiation flux (W m^{-2}) averaged for the time period from August 10, 2015 at 0000 UTC to August 16, 2015 at 0000 UTC for the different WRF-Chem simulations, namely (a) control simulation (M2.04), (b) activity factors (γ_i) updated (MG), (c) PFTs emission factors updated (MGPFT), and (d) the isoprene emission factor updated (M2.10).

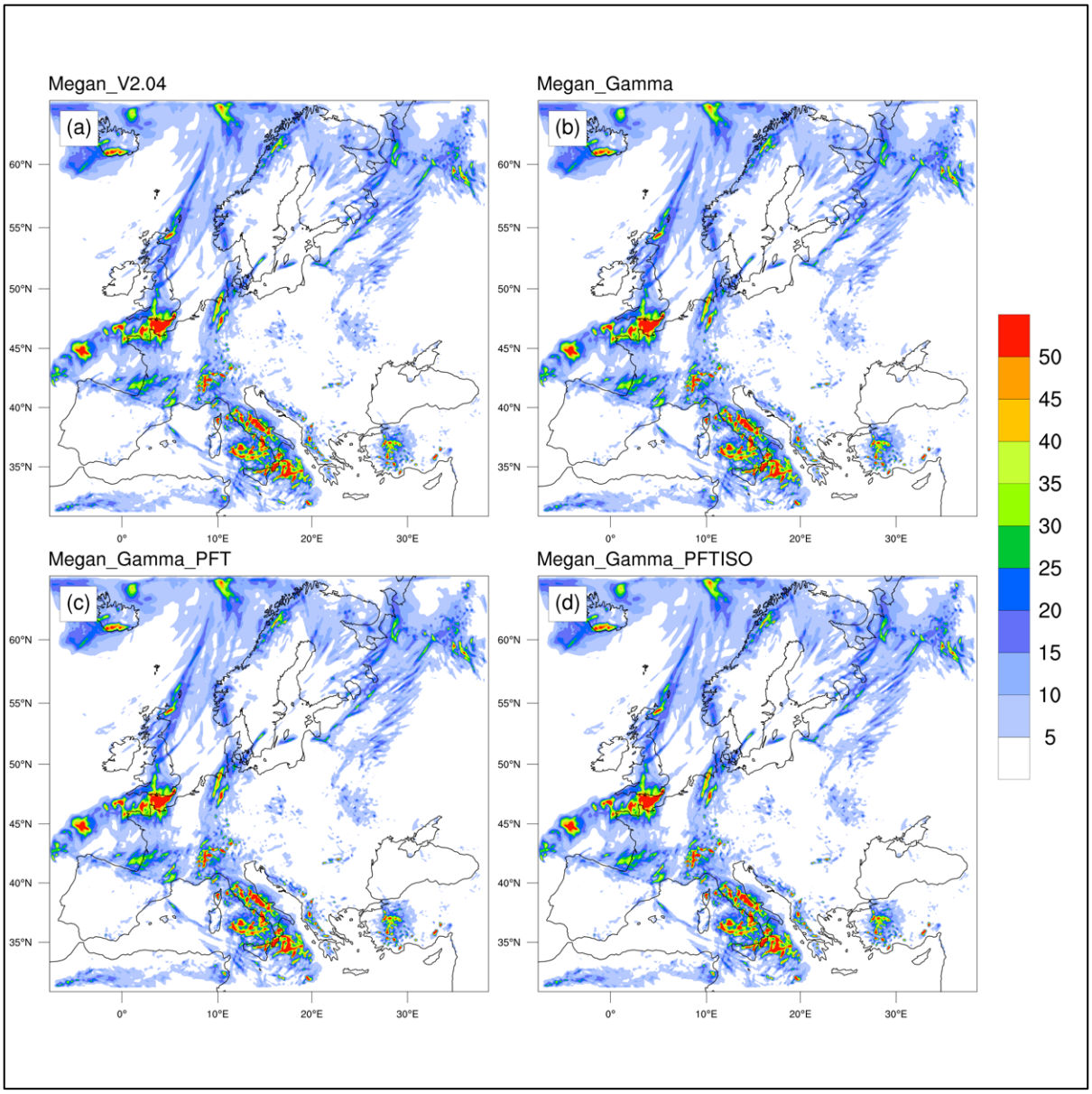

Figure S2: Total precipitation (mm) averaged for the time period from August 10, 2015 at 0000 UTC to August 16, 2015 at 0000 UTC for the different WRF-Chem simulations, namely (a) control simulation (M2.04), (b) activity factors (γ_i) updated (MG), (c) PFTs emission factors updated (MGPFT), and (d) the isoprene emission factor updated (M2.10).

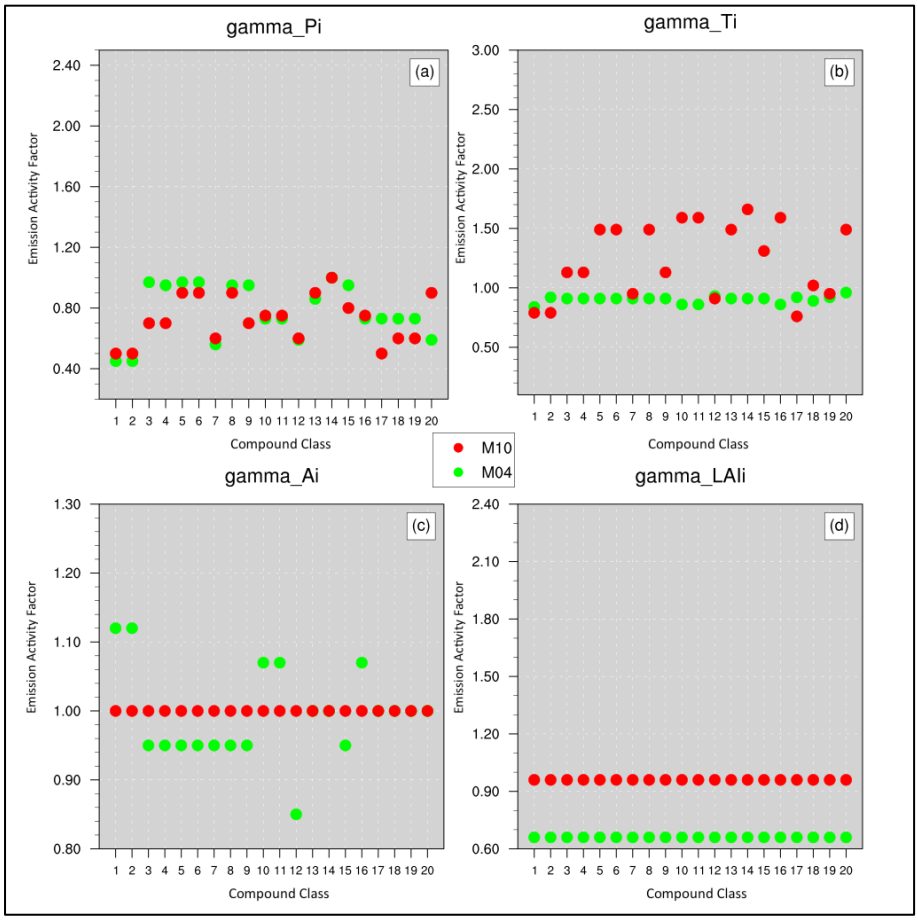

Figure S3: Emission activity factors (y-axis, dimensionless) from M2.04 (M04) and M2.10 (M10) for different compound classes (1. Isoprene, 2. Myrcene, 3. Sabinene, 4. Limonene, 5. 3-Carene, 6. t-β-Ocimene, 7. β-Pinene, 8. α-Pinene, 9. Other Monoterpenes, 10. α-Farnesene, 11. β-Caryophyllene, 12. Other Sesquiterpenes, 13. 232-MBO, 14. Methanol, 15. Acetone, 16. Carbon Monoxide, 17. Nitric Oxide, 18. Bidirectional VOC, 19. Stress VOC and 20. other VOC). Each panel is for a different meteorological factor: (a) photosynthetic photon flux density (γ_P, GAMMA_P), (b) temperature (γ_T, GAMMA_T), (c) leaf age (γ_{age}, GAMMA_A), and (d) leaf area index (γ_{LAI}, GAMMA_LAI). The factors refer to the city of Kiev (Ukraine) on August 13th 885 (12:00 UTC), 2015.

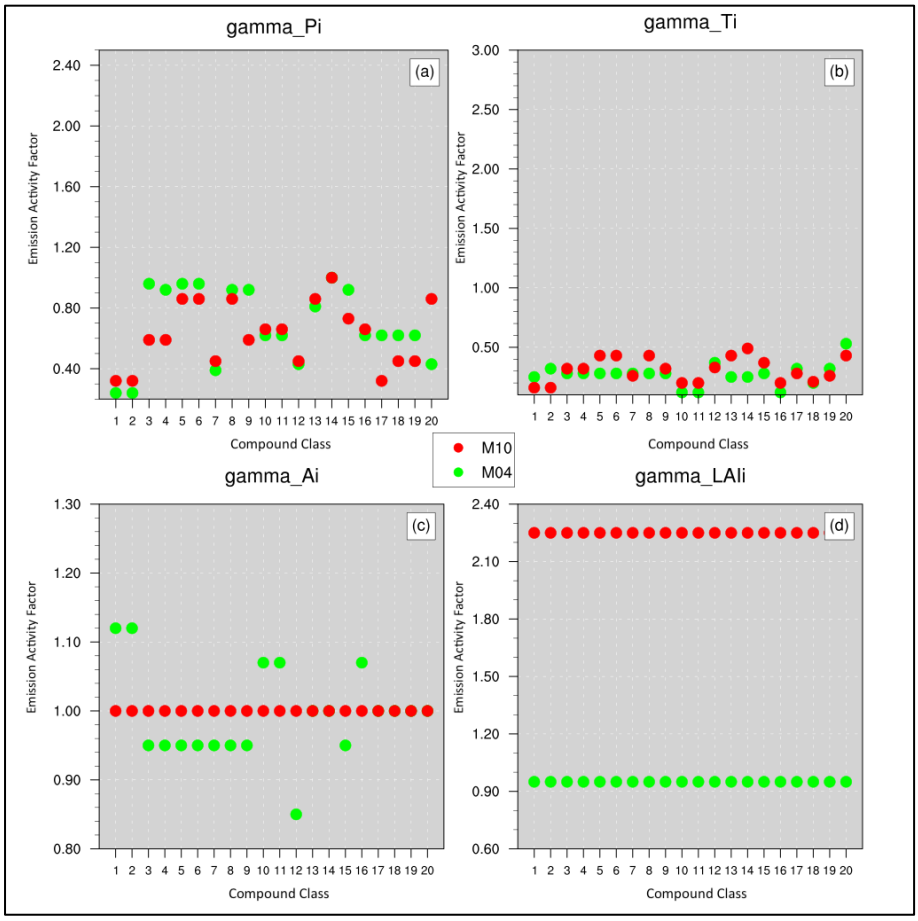

Figure S4: Emission activity factors (y-axis, dimensionless) from M2.04 (M04) and M2.10 (M10) for different compound classes (1. Isoprene, 2. Myrcene, 3. Sabinene, 4. Limonene, 5. 3-Carene, 6. t-β-Ocimene, 7. β-Pinene, 8. α-Pinene, 9. Other Monoterpenes, 10. α-Farnesene, 11. β-Caryophyllene, 12. Other Sesquiterpenes, 13. 232-MBO, 14. Methanol, 15. Acetone, 16. Carbon Monoxide, 17. Nitric Oxide, 18. Bidirectional VOC, 19. Stress VOC and 20. other VOC). Each panel is for a different meteorological factor: (a) photosynthetic photon flux density (γ_P, GAMMA_P), (b) temperature (γ_T, GAMMA_T), (c) leaf age (γ_{age}, GAMMA_A), and (d) leaf area index (γ_{LAI}, GAMMA_LAI). The factors refer to the city of Porto (Portugal) on August 13th 885 (12:00 UTC), 2015.

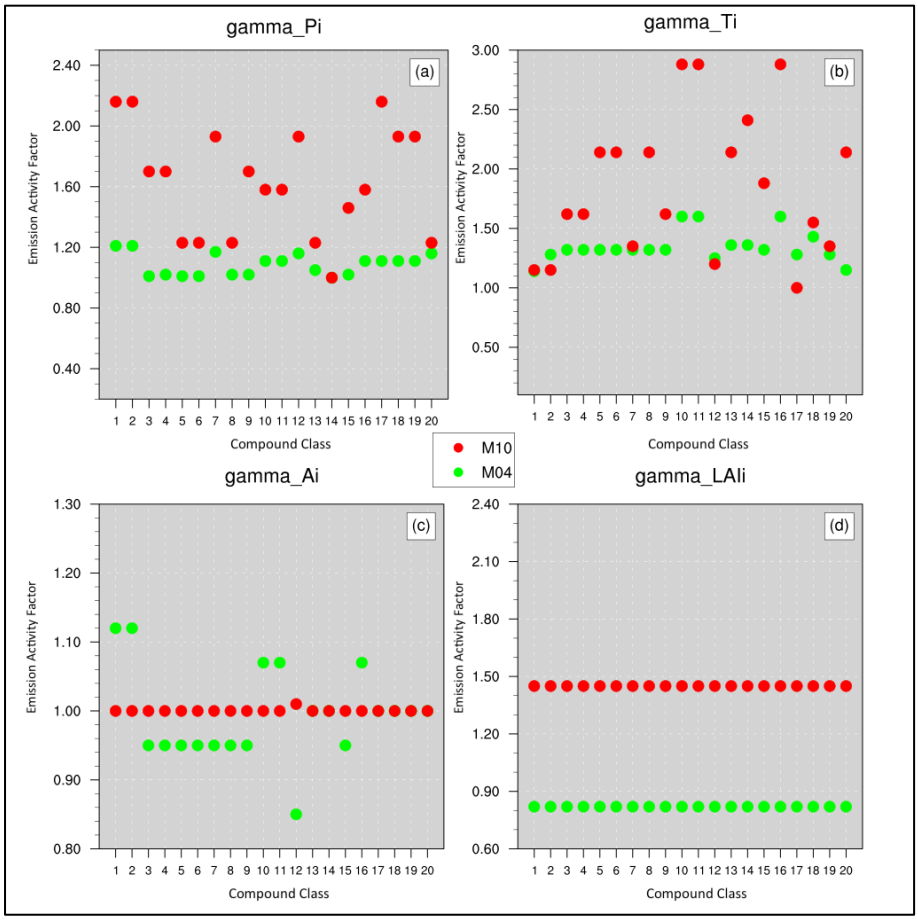

Figure S5: Emission activity factors (y-axis, dimensionless) from M2.04 (M04) and M2.10 (M10) for different compound classes (1. Isoprene, 2. Myrcene, 3. Sabinene, 4. Limonene, 5. 3-Carene, 6. t-β-Ocimene, 7. β-Pinene, 8. α-Pinene, 9. Other Monoterpenes, 10. α-Farnesene, 11. β-Caryophyllene, 12. Other Sesquiterpenes, 13. 232-MBO, 14. Methanol, 15. Acetone, 16. Carbon Monoxide, 17. Nitric Oxide, 18. Bidirectional VOC, 19. Stress VOC and 20. other VOC). Each panel is for a different meteorological factor: (a) photosynthetic photon flux density (γ_P, GAMMA_P), (b) temperature (γ_T, GAMMA_T), (c) leaf age (γ_{age}, GAMMA_A), and (d) leaf area index (γ_{LAI}, GAMMA_LAI). The factors refer to the city of Zagreb (Crotia) on August 13th 885 (12:00 UTC), 2015.

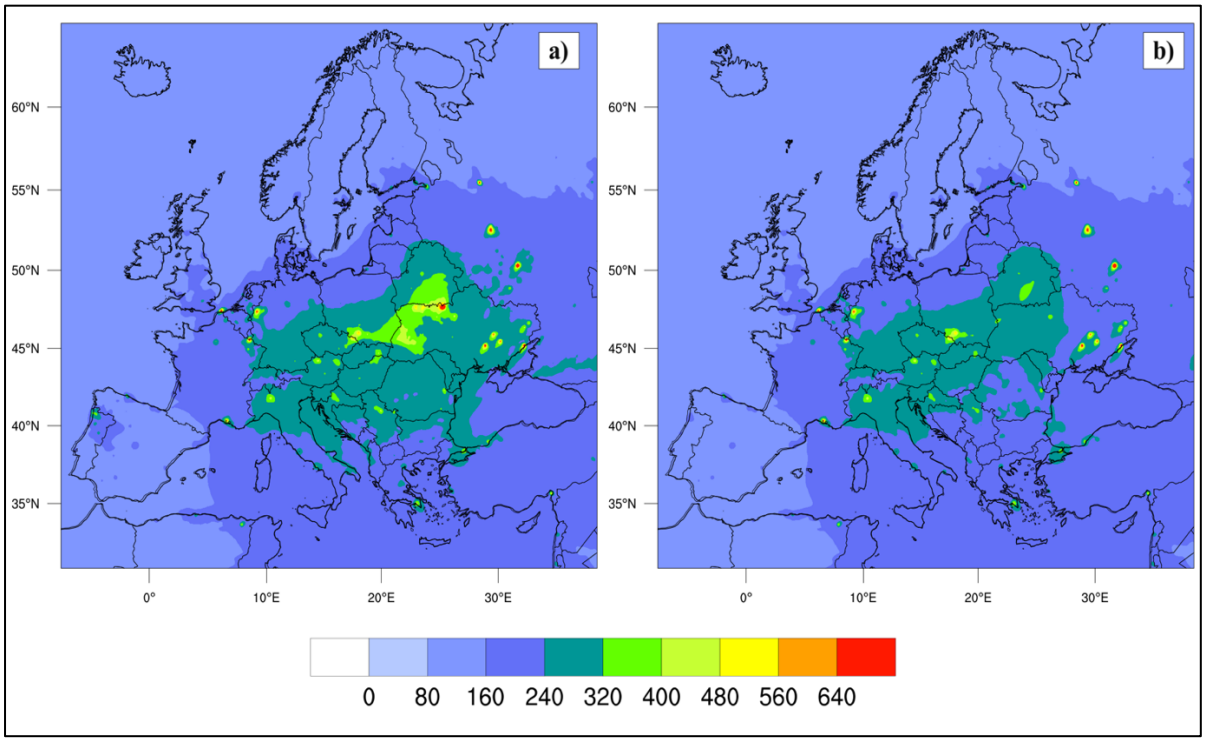

Figure S6: CO concentration (μg m^{-3}) for the simulations (a) with all the MEGAN updates (M2.10 run), and (b) with all the MEGAN updates but without including the biomass burning emissions in the calculation (b - "M10_noFINN"). The maps represent the weekly averages (from August 10th, 2015 at 0000 UTC to August 16th, 2015 at 0000 UTC), extrapolated from WRF-Chem model.

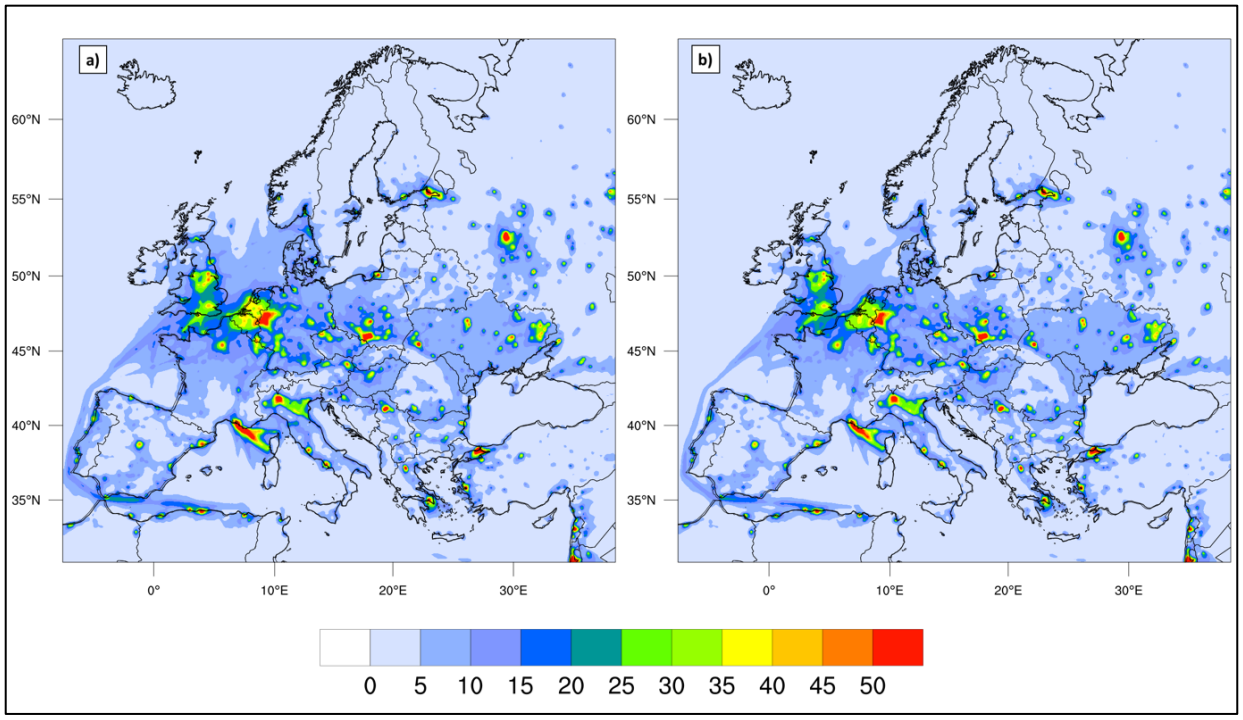

Figure S7: NO2 concentration (µg m-3) for the simulations (a) with all the MEGAN updates (M2.10 run), and (b) with all the MEGAN updates but without including the biomass burning emissions in the calculation (b - "M10_noFINN"). The maps represent the weekly averages (from August 10th, 2015 at 0000 UTC to August 16th, 2015 at 0000 UTC), extrapolated from WRF-Chem model.

Table S2: Gas-phase reactions involving isoprene (ISOP) for the formation of methacrolein (MACR), and methyl vinyl ketone (MVK) in the MOZART-4 chemical mechanism. The table is adapted from Emmons et al., 2010.

Reactants	Products
ISOP + OH	→ $ISOPO_2$
ISOP + O_3	→ 0.4·MACR + 0.2·MVK + 0.07·C_3H_6 + 0.27·OH + 0.06·HO_2 + 0.6·CH_2O + 0.3·CO + 0.1·O_3 + 0.2·MCO_3 + 0.2·CH_3COOH
$ISOPO_2$ + NO	→ 0.08·ONITR + 0.92·NO_2 + HO_2 + 0.55·CH_2O + 0.23·MACR + 0.32·MVK + 0.37·HYDRALD
$ISOPO_2$ + NO_3	→ HO_2 + NO_2 + 0.6·CH_2O + 0.25·MACR + 0.35·MVK + 0.4·HYDRALD
$ISOPO_2$ + HO_2	→ ISOPOOH
ISOPOOH + OH	→ 0.5·XO_2 + 0.5·$ISOPO_2$
$ISOPO_2$ + CH_3O_2	→ 1.2·CH_2O + 0.19·MACR + 0.26·MVK + 0.3·HYDRALD + 0.25·CH_3OH + HO_2
$ISOPO_2$ + CH_3CO_3	→ 0.6·CH_2O + 0.25·MACR + 0.35·MVK + 0.4·HYDRALD + CH_3O_2 + HO_2 + CO_2
ISOP + NO_3	→ $ISOPNO_3$
$ISOPNO_3$ + NO	→ 10.206·NO_2 + 0.072·CH_2O + 0.167·MACR + 0.039·MVK + 0.794·ONITR + 0.794·HO_2
$ISOPNO_3$ + NO_3	→ 10.206·NO_2 + 0.072·CH_2O + 0.167·MACR + 0.039·MVK + 0.794·ONITR + 0.794·HO_2
$ISOPNO_3$ + HO_2	→ 0.206·NO_2 + 0.008·CH_2O + 0.167·MACR
ISOPOOH + hν	→ 0.402·MVK + 0.288·MACR + 0.69·CH_2O + HO_2
TERPOOH + hν	→ OH + 0.1·CH_3COCH_3 + HO_2 + MVK + MACR

Table S3: Summary of the statistics between predicted and measured ozone, isoprene, methyl vinyl ketone (MVK), and methacrolein (MACR), namely the (a) normalized mean bias (bias - %), (b) normalized root mean square errors (nrmse – dimensionless), (c) the correlation coefficient (r - dimensionless), and the relative number of points analyzed (n_{XY}). Values are shown according to the different NOMADSS flights (i.e., rf01, rf02, rf03, rf04, and rf05), and WRF-Chem model runs (M2.04, and M2.10).

		rf01		rf02		rf03		rf04		rf05	
		M2.04	M2.10	M2.04	M2.10	M2.04	M2.10	M2.04	M2.10	M2.04	M2.10
O_3	nxy	254	254	385	385	395	395	237	237	268	268
	nrmse	29.8	30.0	36.3	42.4	24.7	26.4	36.0	42.7	22.5	27.0
	r	0.8	0.8	-0.5	-0.7	0.2	0.0	-0.6	-0.6	0.2	-0.2
	bias	-13.4	-11.5	24.3	30.4	-3.6	2.0	22.6	31.4	7.8	11.9
Isoprene	nxy	88	88	162	162	168	168	121	121	59	59
	nrmse	161.3	128.4	59.8	500.3	97.3	427.9	78.4	697.9	274.8	1677.6
	r	0.2	0.6	0.6	0.6	0.4	0.3	0.5	0.6	0.4	0.5
	bias	-85.1	4.3	27.1	437.7	26.2	298.5	41.6	621.8	203.6	1485.2
MVK	nxy	118	118	164	164	178	178	126	126	64	64
	nrmse	131.4	115.4	61.0	73.8	53.6	45.5	64.4	31.1	40.0	159.9
	r	0.2	0.3	0.6	0.4	0.5	0.5	0.8	0.8	0.7	0.9
	bias	-86.7	-10.3	-39.6	35.6	-41.1	17.7	-56.8	12.3	-22.3	147.1
MACR	nxy	118	118	164	164	174	174	124	124	60	60
	nrmse	129.2	428.4	113.3	565.9	136.4	440.1	99.8	697.1	223.1	1397.4
	r	0.3	0.2	0.6	0.3	0.3	0.4	0.8	0.8	0.6	0.8
	bias	-64.7	204.6	87.2	493.8	95.5	382.8	79.8	645.8	178.0	1295.9

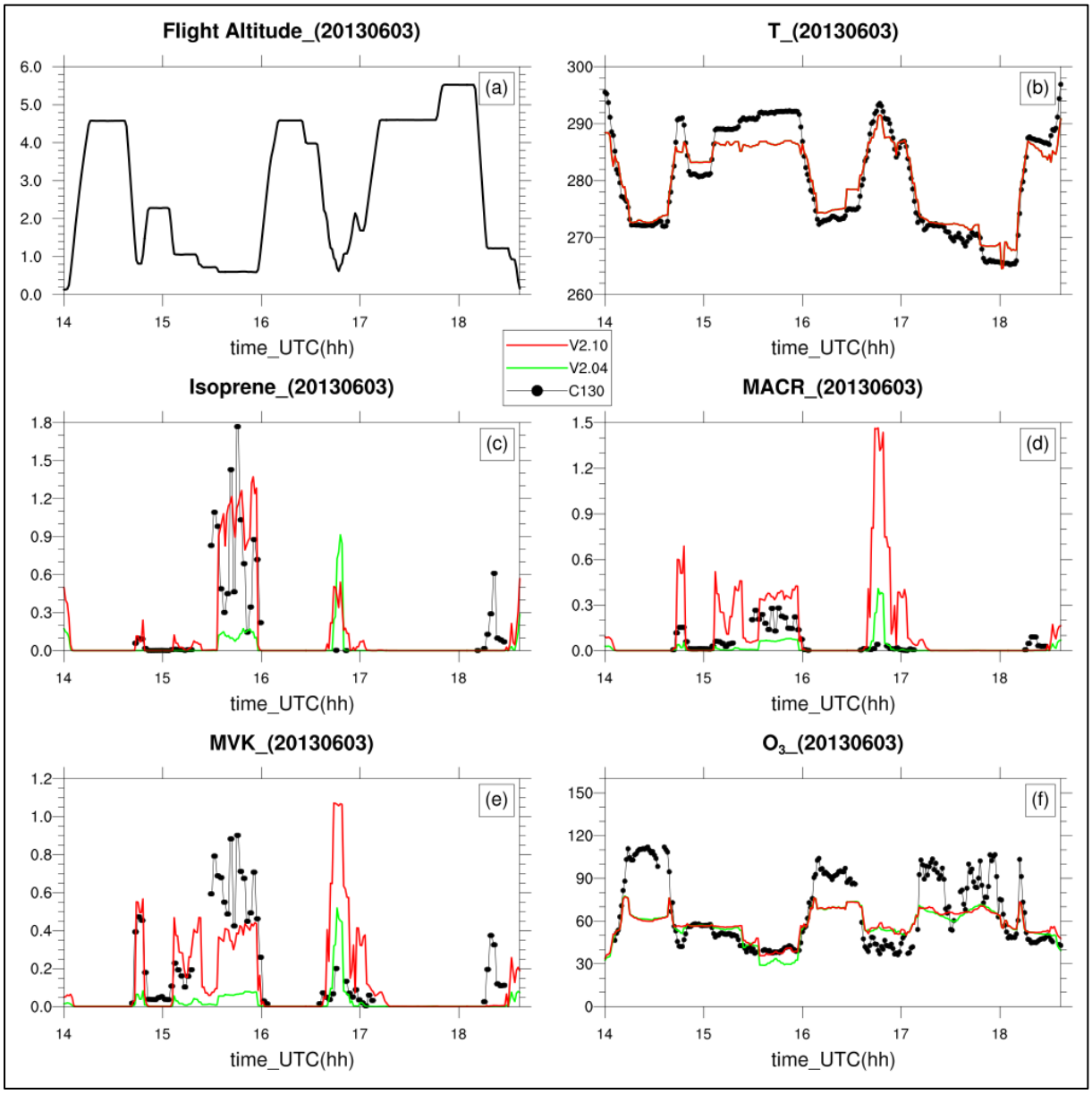

Figure S8: The flight altitude (a - km), the temperature (b - K), the concentration of isoprene (c - ppb), methacrolein (MACR) (d - ppb), methyl vinyl ketone (MVK) (e – ppb), and ozone (f - ppb), for the first NOMADSS flight (rf01). The black line shows the C-130 aircraft measurements, the green and red lines indicate the WRF-Chem model results using MEGAN version 2.04 (M2.04 run) and MEGAN updated to the version 2.10 (M2.10 run), respectively. In the panel b) the green line is not showed since it is overlapped by the red line, they have identical values.

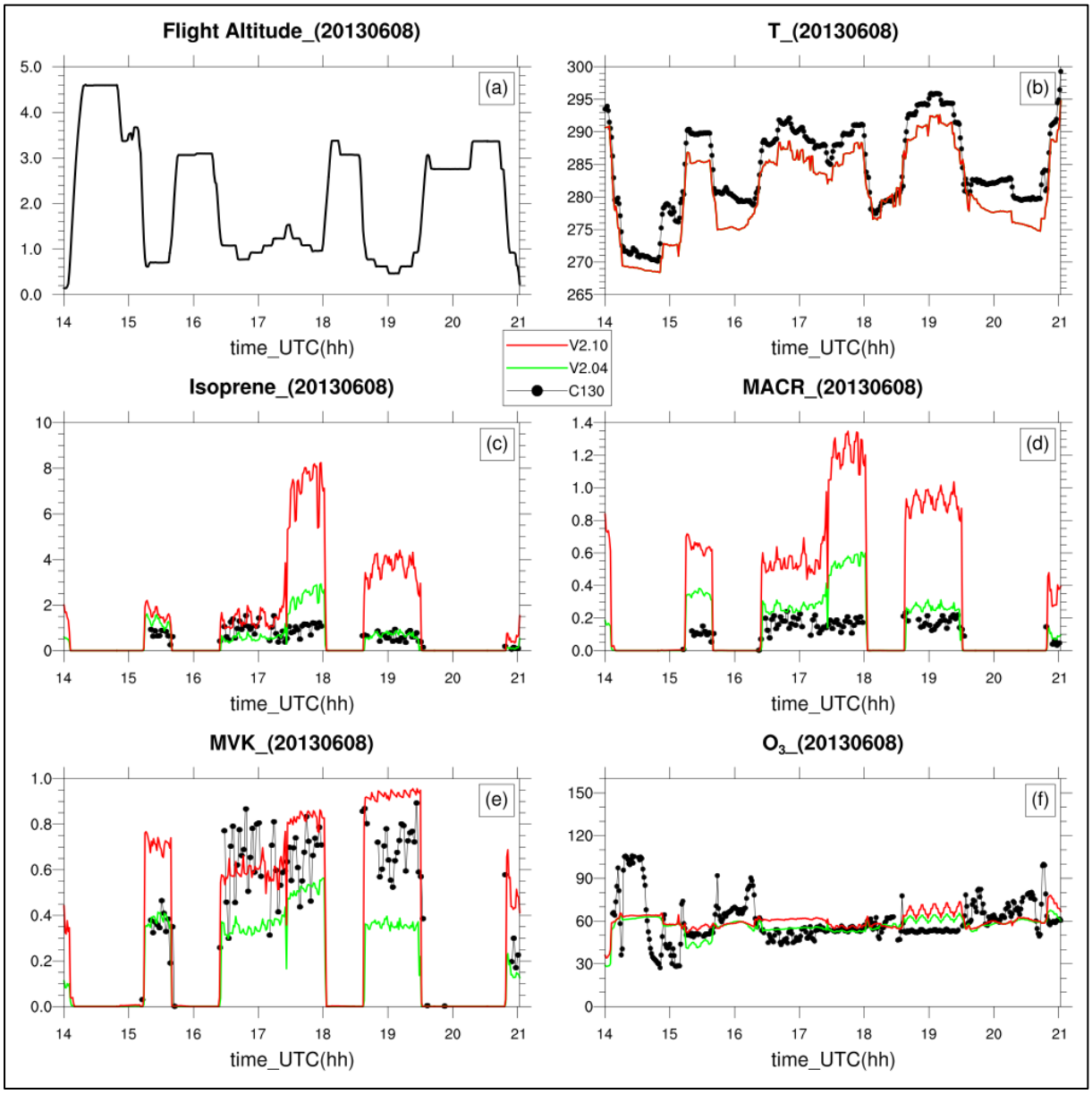

Figure S9: The flight altitude (a - km), the temperature (b - K), the concentration of isoprene (c - ppb), methacrolein (MACR) (d - ppb), methyl vinyl ketone (MVK) (e – ppb), and ozone (f - ppb), for the third NOMADSS flight (rf03). The black line shows the C-130 aircraft measurements, the green and red lines indicate the WRF-Chem model results using MEGAN version 2.04 (M04 run) and MEGAN updated to the version 2.10 (M10 run), respectively. In the panel b) the green line is not showed since it is overlapped by the red line, they have identical values.

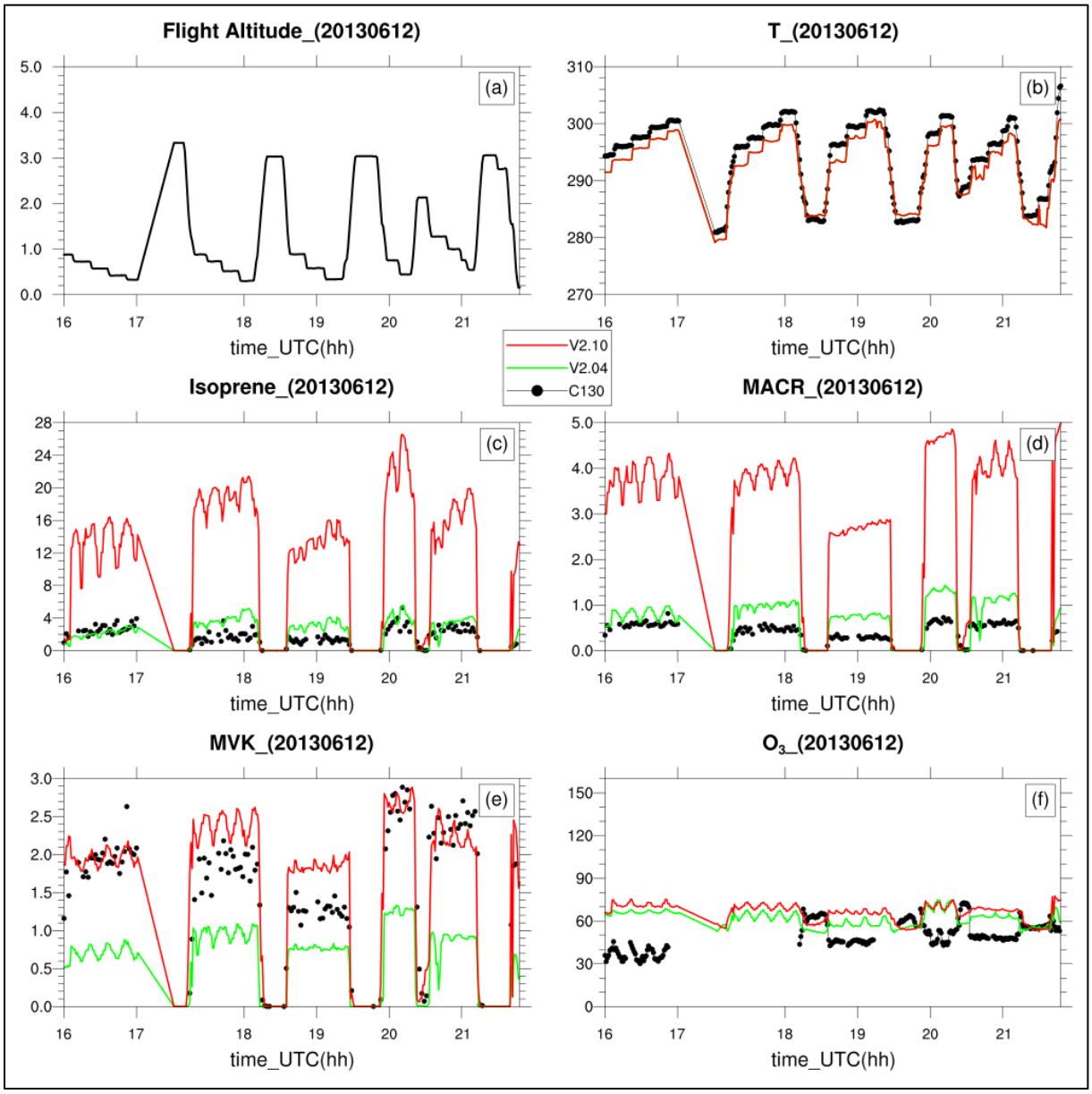

Figure S10: The flight altitude (a - km), the temperature (b - K), the concentration of isoprene (c - ppb), methacrolein (MACR) (d - ppb), methyl vinyl ketone (MVK) (e – ppb), and ozone (f - ppb), for the fourth NOMADSS flight (rf04). The black line shows the C-130 aircraft measurements, the green and red lines indicate the WRF-Chem model results using MEGAN version 2.04 (M04 run) and MEGAN updated to the version 2.10 (M10 run), respectively. In the panel b) the green line is not showed since it is overlapped by the red line, they have identical values.

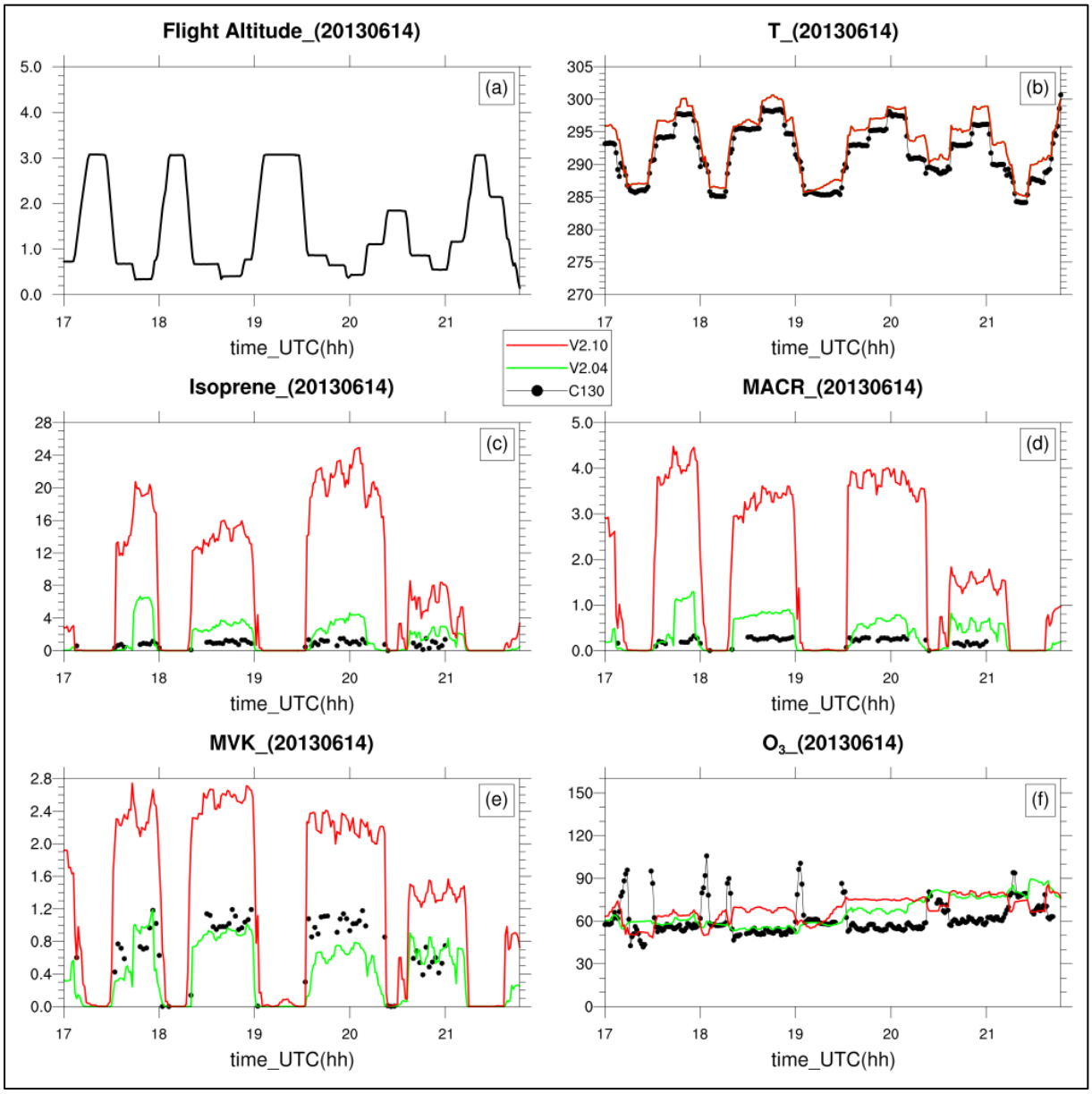

Figure S11: The flight altitude (a - km), the temperature (b - K), the concentration of isoprene (c - ppb), methacrolein (MACR) (d - ppb), methyl vinyl ketone (MVK) (e – ppb), and ozone (f - ppb), for the fifth NOMADSS flight (rf05). The black line shows the C-130 aircraft measurements, the green and red lines indicate the WRF-Chem model results using MEGAN version 2.04 (M04 run) and MEGAN updated to the version 2.10 (M10 run), respectively. In the panel b) the green line is not showed since it is overlapped by the red line, they have identical values.